NTRD Program Disclaimers

1. Disclaimer of Endorsement:

The posting herein of progress reports and final reports provided to TCEQ by its NTRD Grant Agreement recipients does not necessarily constitute or imply an endorsement, recommendation, or favoring by TCEQ or the State of Texas. The views and opinions expressed in said reports do not necessarily state or reflect those of TCEQ or the State of Texas, and shall not be used for advertising or product endorsement purposes.

2. Disclaimer of Liability:

The posting herein of progress reports and final reports provided to TCEQ by its NTRD Grant Agreement recipients does not constitute by TCEQ or the State of Texas the making of any warranty, express or implied, including the warranties of merchantability and fitness for a particular purpose, and such entities do not assume any legal liability or responsibility for the accuracy, completeness, or usefulness of any information,apparatus, product, or process disclosed, or represent that its use would not infringe privately owned rights.

New Technology Research & Development Program
Grant Contract 582-5-65591-0002

Task 1-7 Deliverables Report
Final Report

The preparation of this report is based on work funded in part
by the State of Texas through a Grant from the
Texas Commission on Environmental Quality.

New Technology Research & Development Program
Grant Contract 582-5-65591-0002

High-Temperature Nanocomposite Membranes for Hydrogen Production for Fuel Cells

Final Report

August 30, 2006

The preparation of this report is based on work funded in part
by the State of Texas through a Grant from the
Texas Commission on Environmental Quality.

1. Project Objectives

The overall goal of this project was to develop cost-effective, high-temperature gas separation membranes for producing inexpensive, high-purity hydrogen (H_2) from synthesis gas generated by steam reforming or gasification of fossil fuels. Availability of low-cost hydrogen will facilitate utilization of fuel cells in light- and heavy-duty vehicles as well as in power generation systems to virtually eliminate pollution from these sources and to meet the long-term goals of the New Technology Research and Development (NTRD) program. The proposed technology development will also allow H_2 to be produced from energy sources native to the State of Texas (e.g., natural gas). The project had two specific technical objectives:

(i) To develop polymeric and/or polymer-based nanocomposite membranes with high H_2 permeability, high H_2/carbon monoxide (CO) and H_2/carbon dioxide (CO_2) selectivities, and high thermal stability up to 250-300 °C, the temperature regime for the low-temperature water gas shift reaction process.

(ii) To determine the technical and economic feasibility of using such membranes for producing low-cost fuel-cell-quality H_2 from synthesis gas streams.

2. Project Summary

A series of highly thermally stable polymer films was prepared from polymers that are among the most thermally stable polymeric materials known. We explored the possibility of including a variety of nanoparticles in these polymers to prepare nanocomposite films. We determined the effective combinations of polymers and particles that gave rise to enhanced permeability effects. We characterized the polymers and nanocomposite film thermal stability properties to identify materials that were stable at conditions similar to those of the exit from the water gas shift reactor in a typical process train used to produce hydrogen from fossil fuels, such as coal. We determined that the presence of nanoparticles in poly(benzimidazole) (PBI) did not result in a decrease in thermal stability of the films, which was a significant finding. Moreover, we discovered certain combinations of nanoparticles that, when dispersed in PBI, actually improved its thermal stability in the presence of syngas containing H_2S. The permeation characteristics in both pure gas measurements and mixed gas measurements using relevant mixtures of H_2, CO, CO_2 and H_2S were performed at temperatures up to 300°C on the best samples identified based on there thermal stability properties. We did achieve membranes that exhibited H_2/CO_2 selectivities in the range of 20 at 300°C and H_2/CO selectivities in the range of 35 at the same temperature. This combination of properties is considered good and is among the highest values reported for these gas pairs at such high temperatures. It should be noted that these results were achieved after screening a wide variety of polymers and polymer-based nanocomposites and after considerable effort was made to convert dense, thick films of polymers to relatively thin composite membranes. An economic analysis shows that the polymer membrane supported on a steel microporous support, which was the configuration considered in this study, would have significantly higher cost in practice than DOE's target for the cost of producing hydrogen using membranes. However, most of the cost comes from the current commercial cost of the steel microporous support. If an all-polymer membrane module could be developed, these cost estimates are likely to decrease dramatically.

3. Introduction and Background

Hydrogen is the cleanest burning fuel. Hydrogen-powered automobiles using fuel-cell-based engines have the potential to virtually eliminate emission of all pollutants, including nitrogen oxides (NO_x), particulates, carbon monoxide (CO), and volatile organic chemicals (VOCs), from automobiles.

Fuel cells are also attractive for clean power generation at small, distributed facilities as well as for emergency backup and portable power generation.

A key requirement for transition to fuel-cell-based power generation is availability of inexpensive yet highly pure hydrogen. In the near term, hydrogen must be produced from fossil and biomass fuels by reforming or gasification processes. In a typical process, hydrogen is produced by steam reforming of hydrocarbons at 800-1,000 °C to yield a synthesis gas stream consisting mainly of H_2 and CO. The CO in this stream is then converted to additional H_2 by reacting it with steam in a two-step water gas shift (WGS) reaction process typically conducted at 400 and 250 °C, respectively. Because H_2 supplied to fuel cells must be high-purity, the hot H_2 stream must be purified to separate it from other synthesis gas components, such as CO and CO_2. In particular, the H_2 fuel should have <10 ppm CO because CO hurts the efficiency of the catalyst used in fuel cells. Separation of H_2 from CO_2 is also desirable to allow CO_2 capture followed by its long-term sequestration in depleted oil and gas reservoirs, deep saline aquifers, or other suitable geological formations.

Inorganic membrane materials, such as zeolites, carbon, and silica, have been considered for high-temperature separation environments[1] because of their have excellent thermal stability in the temperature ranges of interest to this work. However, they are mechanically very fragile. Furthermore, it has not proven possible thus far to package such materials into the high surface area/volume ratio membrane modules required for this application. From a practical viewpoint, such inorganic materials do not appear to provide viable separation membranes in the foreseeable future.

Commercial polymeric gas separation membranes can also be used to selectively remove H_2 from CO_2 and CO in synthesis gas streams. However, these membranes are made from conventional polymers (e.g., polysulfone) that do not have the thermal stability to be used in application temperatures much above 90 °C, much less at the lower water-gas-shift reaction temperature of 250-300 °C. On the other hand, most thermally stable polymers are very impermeable materials, rendering them impractical for gas separation membrane applications because of the high capital costs associated with producing the very large membrane surface areas needed to achieve desired gas production levels. The extraordinarily low permeability values of highly thermally stable polymers have thus discouraged exploration of the gas separation properties of such materials. Little is therefore known of the separation properties of highly thermally stable polymers, and there are no systematic data regarding their separation performance at the high temperatures of this application.

This project was initiated to investigate in a systematic manner the high-temperature H_2 separation performance of several selected, highly thermally stable polymers and their nanocomposites formed by physically dispersing nano-sized filler particle into these polymer matrices and to develop high-performance, high-temperature membrane technology based on such polymers for high-purity H_2 production. A number of high-temperature-resistant, organic polymers do exist. Many of these polymers have highly aromatic, rigid chemical structures and exhibit decomposition temperatures exceeding the 250-300 °C requirement of the low-temperature WGS process temperature. Table 1 shows the candidate high-temperature polymers that appeared potentially attractive as gas separation membranes and were hence studied in this project. The majority of the project work focused on unfilled PBI because this commercial polymer has recently been reported to be highly selective for H_2 at 250-300 °C (e.g., H_2/CO_2 selectivity greater than 20).[2] The other aromatic polymers and their nanofilled composites were examined as possible alternatives that might show comparable or better properties than PBI. The nanofilled polymer membrane approach is based on the recent discovery that addition of nanoscale, nonporous particles into very rigid polymer matrices unexpectedly results in significant increases in permeability by actually increasing the polymer free volume available for gas permeation.[3,4] Because the permeability enhancement also increases with decreasing permeability of the polymer matrix,[3] it seemed logical that the inherently low-permeability, thermally stable polymers in Table 1 would be quite susceptible to this

permeability-enhancing nanocomposite effect. Hence, the nanofilled polymer membrane approach was used as an attempt to effect an enhancement of the gas permeability of the candidate, high-temperature polymers without sacrificing too much of their selectivity for H_2 over other syngas components (e.g., CO, CO_2). If highly thermally stable polymers having high H_2 permeability and excellent H_2/CO and H_2/CO_2 separation properties at 250-300 °C could be prepared, a breakthrough in membrane performance and process economics would occur for high-temperature membrane-based separations. If the gas streams could be separated at process conditions, the cost of producing H_2 for fuel-cell-based power generation would be markedly reduced. Moreover, capturing CO_2 at high pressure would lower the cost of CO_2 sequestration, providing strong economic stimulus for this approach.

Table 1. Highly Thermally Stable Polymers Studied

Name	Structure	T_g (°C)*	T_d (°C)*
Polybenzimidazole [PBI]	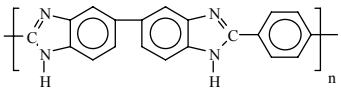	>430	650
Polybenzoxazole [PBO]	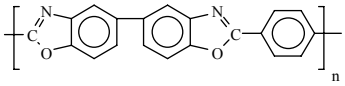	330	620
Polyimide [PI] (Matrimid® 5218 shown)	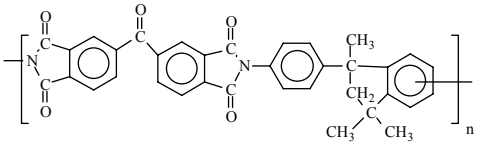	338	585
Poly(ether imide) (Ultem® 1000 shown)	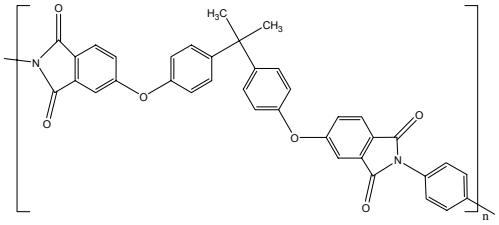	209	522
Poly(amide imide) (Torlon® AI-10 shown)	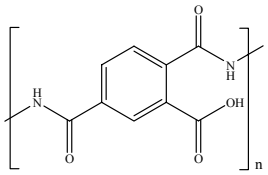	272	>315

* $T_g \equiv$ polymer glass transition (softening) temperature; $T_d \equiv$ polymer decomposition temperature.

In this project, we prepared free-standing membrane films, with and without nanofillers, from the selected thermally stable polymers and conducted a series of permeation tests on these films with pure gases (e.g., H_2, CO_2) and syngas mixtures to systematically explore their intrinsic gas separation properties as a function of temperature (up to 300 °C) and feed pressure (up to 300 psig). These permeation studies also provided the information needed to determine the potential of these polymer membrane materials for high-temperature H_2 separation applications. In addition to the dense membrane films, thin-film, composite PBI membranes supported on microporous, stainless steel substrates were also

evaluated in permeation tests to determine how much the H_2 flux (productivity) can be improved by using this substrate approach to mechanically support a very thin, defect-free, selective PBI layer. Furthermore, we characterized the thermal decomposition (i.e., thermal stability) behavior of the base polymers and their nanocomposites in not only an inert helium atmosphere but also a simulated syngas environment to more realistically evaluate the membrane thermal stability under gas conditions close to those of the actual process. Using the experimental separation performance data collected in the laboratory, a membrane process design for generating 10 L/min of hydrogen from syngas was prepared, and technical and economic analyses of this process were performed.

4. Experimental

4.1. High-Temperature Membrane Preparation

UT

Nanoparticles

MgO Plus (Nanoscale, Manhattan, KS) was used in this study. According to the supplier, these MgO nanoparticles have a BET surface area between 600 and 680 m^2/g. The resulting average equivalent spherical particle diameter is 3 nm, where equivalent spherical particle diameter is defined as 6/(surface area x density). Samples are reported to be spherical, and the metal composition is 99.2% pure Mg, with the remainder being trace impurities. SiO_2 nanoparticles were obtained from Sigma-Aldrich. These samples are reported to be spherical aerogels with a primary particle diameter of 10 nm. The MgO and SiO_2 nanoparticles have been selected as inert particles which should not react with the penetrant gases.

Zn and Ni nanoparticles were obtained from RTI. The Zn nanoparticles have been selected due to their potential to act as a water gas shift (WGS) catalyst in the polymer matrix. The Ni nanoparticles have been selected for their potential as CO hydrogenation catalysts. All nanoparticle samples were used as received. The particle composition, primary particle diameter, and expected particle reactivity are presented in Table 2.

Table 2. Candidate Nanoparticle Materials

Nanoparticle	Primary particle diameter (nm)	Expected particle reactivity
MgO	3	Neutral
SiO_2	10	Neutral
Zn	20	WGS catalyst
Ni	20	CO hydrogenation catalyst

Polymer: Two highly thermally stable polymers were selected as polymer membrane matrix candidates for this project. Torlon AI-10 (i.e., poly(amic acid)) was obtained from Solvay Advanced Polymers (Alpharetta, GA) and used as received. Ultem 1000 (i.e., poly(etherimide)) was obtained from General Electric Co. and was used as received. The structures for both materials and their respective glass transition temperatures are presented in Table 1.

Torlon AI-10 Film Preparation

Attempts were made to solution-cast Torlon AI-10 filled with MgO and SiO_2 nanoparticles. According to the supplier, dimethylacetimde is a solvent for Torlon AI-10.[5] Films were prepared by adding 1.5 grams of Torlon AI-10 to 30 grams of dimethylacetimde and allowing the polymer to dissolve completely while mixing with a magnetic stir rod. Both MgO and SiO_2 nanoparticles were added to the polymer solution at a predetermined volume fraction, ϕ_F, which was calculated as follows:

$$\phi_F = \frac{W_F / \rho_F}{\left(W_P / \rho_P + W_F / \rho_F\right)} \tag{1}$$

where W_F and W_P are the masses of filler and polymer in the sample, respectively; ρ_F and ρ_P are the densities of pure filler and pure polymer, respectively. The density of Torlon AI-10 is 1.12 g/cm^3. The MgO and SiO_2 densities are 3.6 g/cm^3 and 2.2 g/cm^3, respectively. After mechanically mixing the particles using a magnetic stir bar, the particle filled solution was cast in a vented casting plate until the solvent was removed, which usually required 1 to 2 days.

MgO and SiO_2 Filled Ultem 1000 Nanocomposite Membrane Preparation:

Ultem 1000 films were prepared by adding 1.5 grams of Ultem 1000 to 30 of grams methylene chloride or chloroform. The polymer was given sufficient time to dissolve completely while being stirred with a magnetic stir rod. Both MgO and SiO_2 nanoparticles were added to the polymer solution at a predetermined volume fraction, as calculated by Eq. (1). The density of Ultem 1000 is 1.26 g/cm^3. After mechanically mixing the particles using a magnetic stir bar, the particle filled solution was cast onto a vented casting plate until the solvent was removed. The casting plate was coated with Teflon or aluminum tape to facilitate the removal of the cast film from the casting plate.

Ni and Zn filled Ultem 1000 Nanocomposite Membrane Preparation

Films of Ultem 1000 filled with either Ni or Cu have been prepared with a predetermined volume fraction nanoparticle as calculated by Eq. (1). The density of the Ni and Cu nanoparticles was 8.99 g/cm3, as estimated by the density of similar nanoparticle available commercially.

Copper nanoparticles have been dispersed in an Ultem 1000 film. The Cu nanoparticles were dispersed into solution by vigorously shaking the particle filled solution by hand for 1 minute, ultrasonicating the solution for 20 minutes, and then vigorously shaking the sample while it was transported from the ultrasonicator to the casting plate. This method prevented the particles from settling before the sample was cast. It is believed that the solvent evaporates sufficiently quickly to prevent particle settling.

RTI

Membrane Casting Solutions

Viscous membrane casting solutions were prepared from a bronze, 100-mesh (sub-149-µm) Celazole® polybenzimidazole (PBI) powder purchased from Celanese Advanced Materials, Inc. (CAMI, Charlotte, NC). The PBI casting solutions with the best viscosities for membrane film preparation

contained 10-15 wt% polymer in *N,N*-dimethylacetamide (DMAc). They were made by mechanically stirring the polymer/solvent mixtures for 3-5 h at 150-170 °C in a silicone oil heating bath.

PBI nanocomposite membranes were also prepared from PBI casting solutions doped with various nanoparticles. The nanofiller types used were two different nanosilicas and a type of highly dispersed, alumina-supported Ni catalyst nanoparticles. One silica type was an untreated, hygroscopic SiO_2 nanopowder from Aldrich (St. Louis, MO). The Aldrich SiO_2 had a 10-nm particle size. The other silica type was hydrophobic Cab-O-Sil® TS-530 (Cabot Corp., Tuscola, IL), which was a fumed silica chemically treated to have nonpolar trimethylsilylated [$-Si(CH_3)_3$] surface groups. The TS-530 silica had a 13-nm primary particle diameter. The nonreactive metal oxide nanoparticles of SiO_2 were chosen due to their commercial availability. Because of the acidic nature of such metal oxides, the SiO_2 nanoparticles do not adsorb acid gases such as CO_2 and, hence, should be inert to CO_2. The Ni catalyst supported on alumina was synthesized in-house at RTI. The Ni/Al_2O_3 catalyst sample used in this project was pre-reduced at 450 °C for 3 h in 100% H_2 and passivated in 1% O_2/N_2 at room temperature. Ni nanoparticles are catalytically active and are known to react with CO under conditions similar to those of the low-temperature WGS reaction, making them a suitable nanofiller candidate for this project. Table 3 presents the physicochemical properties of the Ni/Al_2O_3 catalyst.

Table 3. Physicochemical Properties of Highly Dispersed Ni/Al_2O_3 Catalysts

Sample code	Ni specific surface area (m^2/g Ni)	Ni dispersion (%)	Ni crystallite size (nm)
041205a-NiHRP	142.2	21.4	5.2

Casting solutions for making PBI/silica nanocomposite membranes were made by first predispersing premeasured amounts of the nanoparticles in minimal quantities of DMAc solvent. After stirring for at least 15-24 h, the entire contents of each well-mixed particle/solvent suspension were then added to the corresponding PBI/DMAc solution for which that particular suspension quantity had been premeasured to obtain the desired concentration ratio of filler:polymer. All silica-doped membrane casting solutions were prepared using the 14 and 15 wt% PBI solution in DMAc, which were made as needed for the nanocomposite solutions. To ensure adequate mixing before use, the resulting PBI/nanoparticle/DMAc casting solutions were stirred vigorously for at least 24 h. As an additional precaution to prevent particle settling, the nanoparticle-loaded PBI solutions were stirred up to the time of the membrane casting step.

Membrane Film Preparation

Free-standing PBI-based membrane films were prepared (i) by casting the polymer solutions (doped and undoped with nanoparticles) into casting rings supported on glass plates or (ii) by drawing down these solutions onto glass plates with a doctor blade (knife) set to desired gap clearances. The freshly cast films were placed immediately placed in a 70 °C oven with N_2 purge to dry for 18-24 h. Thickness of the dry films was determined using a digital micrometer readable to ±1 µm. The resulting dry films were a clear golden brown color and flexible. Initially the first technique using casting-rings gave films that were not very flat or uniform. Eventually, though, after a number of attempts and modifying film casting/drying conditions, more robust PBI films could be made via the casting-ring approach. The second method utilizing a casting knife successfully made thinner, more uniform films. Representative knife-cast PBI films are shown in Figure 1. The pure PBI film had a thickness of 6 µm, while the PBI films filled with 10 wt% Aldrich SiO_2 and 10 wt% TS-530 had thicknesses of ~ 8 µm.

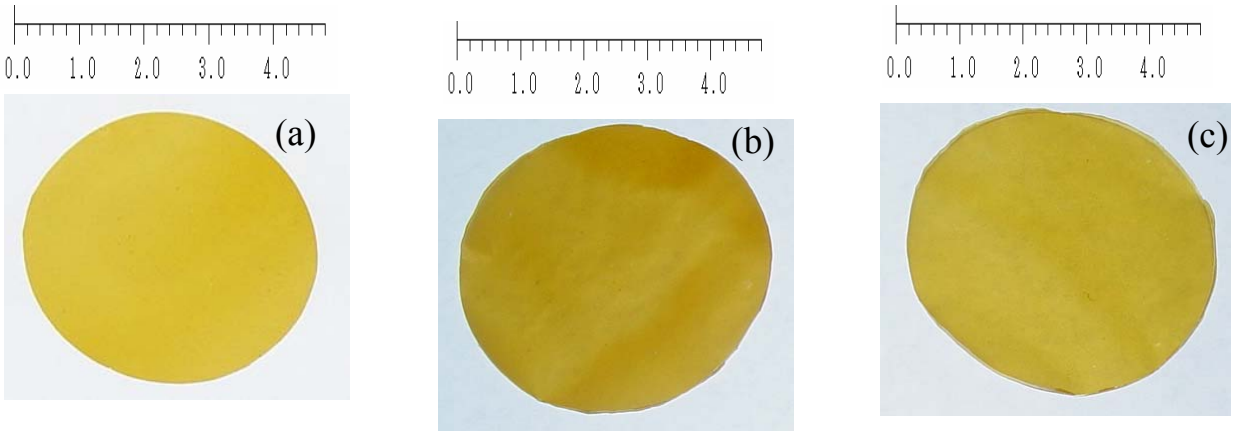

Figure 1. Knife-cast, free-standing, Celazole PBI nanocomposite films doped with (a) 0 wt% nanoparticles, (b) 10 wt% Aldrich SiO_2 particles, and (c) 10 wt% Cab-O-Sil TS-530 fumed silica particles. The pure PBI film was cast with a 4-mil knife gap; the nanocomposite films were cast with a 4.5-mil knife gap. Films were dried for (a) 24 h, (b) 5 h, and (c) 10 h in 70 °C oven with N_2 purge. Scale shown above each photograph has units of centimeters.

Our initial film drying procedure (70-100 °C for 10-24 h) did not effectively remove all solvent and moisture from the PBI-based films. On the basis of thermogravimetric (TGA) studies, roughly 16-20 wt% volatile solvent/moisture remained in the films after the initial drying step, and this leftover solvent/moisture could significantly affect membrane permeation properties. Thus, to drive off this leftover solvent/moisture, the overall film drying protocol was modified to include post-heat treatment steps at 250 °C for 18-20 h and 300-350 °C for a range of times under N_2.

To verify complete moisture/solvent loss, a "dual-scan" TGA procedure made up of two sequential temperature programs was used. In TGA Scan #1, to accelerate removal of residual solvent/moisture, membrane samples were heated and then held isothermally for a given runtime period at an intermediate temperature higher than the boiling points of solvent and moisture. For example, the membrane film was heated in Scan #1 from room temperature to 350 °C, held at 350 °C for 30 min, and cooled to room temperature. The subsequent TGA Scan #2 heated samples from room temperature to 800 °C and held them at this final temperature for 30 min. All TGA scans done during this period were performed in helium and at a 10 °C/min heating rate.

"Proof-of-concept" attempts were also made to make thin-film PBI composite (multilayered) membranes consisting of a much thinner (~1 µm), selective PBI layer supported on a microporous substrate for mechanical strength. Two microporous substrates —an inorganic Anopore™ alumina support and a 316L stainless-steel support with 0.5-µm pore size (Mott Corp.) — were tried. Composite membranes were formed by knife-casting or hand-wicking the polymer casting solutions onto these substrates. The Anopore substrate trials were unsuccessful because this support was too brittle, so it curled and eventually cracked under the drying stresses of the coated PBI layer.

The first PBI coating attempt on a 0.5-µm-pore-size stainless steel substrate used the knife-casting technique with the knife gap essentially zeroed to the substrate thickness. Because the substrate was not perfectly flat, regions existed where the PBI solution coating did not cover the support

surface. Furthermore, after heating at 70 °C for 24 h, most of the PBI layer appeared to absorb into the substrate. The only evidence that a coating had been applied was indicated by a slight darkening of the metal support surface. In our second attempt, a small quantity of PBI solution was poured onto the substrate and coated (spread out) manually to cover the entire support. The resulting coating layer was thicker than that in the first attempt. After drying overnight at 70 °C, a film of PBI was found only on the substrate section where the polymer solution coating had initially been thickest. Another layer of PBI solution was then deposited on top of the first layer. This second PBI layer allowed for complete coverage of the substrate surface after drying so a third PBI coating layer was not applied.

A second 0.5-µm-pore-size stainless steel substrate was coated with PBI casting solution to retry the knife-casting approach with the knife gap essentially zeroed to the substrate thickness. Because this substrate was flatter than the first one, the initial coating was successful for much of the substrate. The knife-gap clearance was increased, and another coating was applied. The second coating appeared to have sufficiently covered the entire substrate area

AccuSep®-Supported PBI Composite Membrane Tubes

For the high-temperature, thin-film composite membrane development work in this project, two PBI composite membranes supported on AccuSep® microporous, stainless-steel tubes were also fabricated by and acquired from Pall Corporation. (AccuSep is a sintered metal substrate available as a small tube that can be packaged into a membrane module with moderate surface area/volume ratio.) The first tubular PBI composite membrane was defective (cf. Results and Discussion). The second one was defect-free and had an apparent PBI layer thickness of 0.65 µm and an effective membrane area of 28.4 cm^2. A photo of the AccuSep-supported PBI composite membrane is shown in Figure 2.

Figure 2. Tubular, AccuSep-supported PBI composite membrane acquired from Pall Corporation.

4.2. Membrane Permeation Tests

UT

Pure Gas Permeability

Pure gas permeation estimates were performed using a constant volume/variable pressure apparatus.[6,7] Films were masked with aluminum tape. The constant volume/variable pressure apparatus was exposed to a vacuum for at least 24 hours to evacuate gas from the chamber and remove any residual gas from the sample film. Prior to testing the films were exposed to the test gas at 3.4 atm upstream pressure for at least two hours to ensure that steady state permeation was established. Gas permeability (cm^3(STP) cm/(cm^2 s cmHg)) was calculated from the steady state pressure change in the downstream volume according to [6,7]

$$P_A = \frac{V}{RT}\frac{l}{Ap_{atm}}\frac{dp}{dt} \tag{2}$$

where V is the downstream volume (cm^3), dp/dt is the pressure change in the downstream volume (cmHg/s), l is the film thickness (μm), p_{atm} is atmospheric absolute pressure (cmHg), A is the area of the film available for transport (cm^2), R is the gas constant, and T is absolute temperature (K). All experiments were performed at downstream pressure below 1 cmHg.

RTI

Pure-gas and mixed-gas permeabilities in PBI- and other high-temperature polymer membranes were measured using a modified constant-pressure/variable-volume method utilizing a downstream sweep gas. The gas permeation apparatus used is shown in Figure 3. Gas chromatographs were connected to the permeation system to allow online analysis of feed, residue, and permeate stream compositions. Gas permeation properties of the membranes were determined as a function of temperature [20-300 °C] and feed (upstream) pressure [20-300 psig]. In all tests, the permeate (downstream) pressure was 0 psig. Pure-gas permeation experiments were performed with H_2 and CO_2. Nearly all gas mixture experiments were conducted with a ternary syngas composition of 36.8% H_2, 12.5% CO_2, and 50.7% CO. For completeness, the best membrane at the end of these studies was also evaluated with a four-component H_2S-containing syngas mixture (1.02% H_2S, 35.9% H_2, 13% CO_2, and 50.08% CO). Unless noted otherwise, the permeation tests used a downstream helium sweep gas flow rate of 20 cm^3/min. All gas permeabilities are reported in units of barrers, where 1 barrer is 1×10^{-10} $cm^3(STP)\cdot cm/(cm^2\cdot s\cdot cmHg)$.

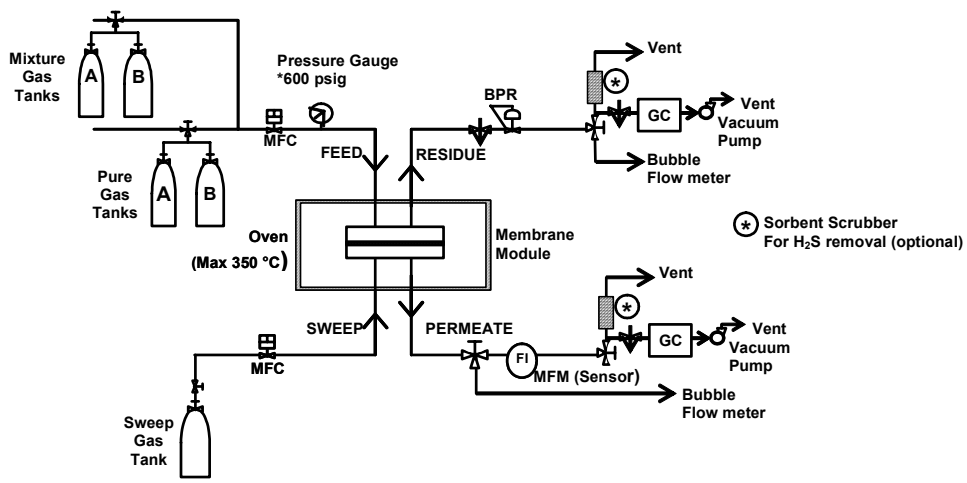

Figure 3. Schematic of modified constant-pressure/variable-volume membrane permeation test system with online GC analysis used at RTI.

An initial permeation testing protocol was developed to measure permeation properties over a feed temperature range of 20 to 250 °C. For the testing of the PBI membranes, initially each pure gas was measured over the entire temperature range. Upon the degradation of many early samples during testing, the permeation testing procedure was modified to counter the defect formation during testing. First, instead of completing each gas with all temperatures, both H_2 and CO_2 were run at a single temperature point before increasing the temperature to ensure selectivity calculations at each temperature. Upon completion of daily permeability values, initially the films would be set up so that the GC was run over night to detect any overnight degradation. It was found that degradation did not occur while gas was

continually running over the film. When returning the permeation cell to room temperature after the full temperature characterization was completed, the descent was done in the same stages as the increase, while testing the permeability at each stage.

For the tubular PBI composite membrane modules examined, the permeation testing protocol was revised for experiments done over the temperature range of 100 to 300 °C. All pure-H_2 data was first collected at 20, 50, 100, 200, and 300 psig feed pressures; CO_2 tests were then conducted at the same pressures. Quality control steps included doing a low pressure check upon completion of the 300 psig run as well as testing H_2 again at various pressures after the CO_2 analysis. After the pure-gas tests, the membrane module were evaluated at room temperature with the ternary syngas mixture at 100, 200, and 300 psig feed pressures. Before moving on to the next temperature point, pure H_2 and CO_2 quality control checks were completed.

A summary of the pure PBI and PBI nanocomposite films evaluated in gas permeation studies is presented in Table 4.

Table 4. Pure PBI and Nanoparticle-Filled PBI Films Tested for Gas Permeation Properties

Polymer Solution Details			Knife-Gap Clearance (-mil)	Thickness (mm)	Drying Conditions			
					Initial Drying		Post-heat treatment	
Sample Name	Additive				Temperature (°C)	Time (h)	Temperature (°C)	Time (h)
	Particle	% wt						
A1	-		GRGP[a]	19	70	24	-	-
A4	-		10	21	70	24	250	24
A5	-		10	13	70	24	350	2
A6	-		10	30	70	24	350	2
B1[b]	-		GRGP[a]	34	70	24	250	24
B2[b]	-		GRGP[a]	35	70	24	250	24
AS2-M	**SiO_2**	**10**	10	9	70	24	250	24
AS3-M			10	18	70	24	-	-
AS4-M			15	21	70	24	300	2
AS5-M			8	13	70	24	300	2
AN-1M	**Ni**	**4.76**	8	16	70	24	300	2
AN-2M			8	16	70	24	300	2

[a] Indicates film was cast using Glass Ring on Glass Plate technique.

[b] These samples were made with Pall Corporation PBI, while all other films were made using Celazole PBI as detailed in Task 1.

4.3. Thermal Characterization of High-Temperature Polymer Membranes

UT

Differential Scanning Calorimetry (DSC)

The thermal behavior for unfilled and SiO_2 filled Ultem 1000 films were characterized using a Q-100 DSC (TA Instruments, New Castle, DE). Samples were prepared by cutting a small section of a film. These sections weighed between 10 and 20 mg. The samples were placed in a DSC pan (TA

Instruments, New Castle, DE) and placed in the DSC chamber. Samples were initially heated from room temperature to 270 °C, which is 60 °C higher than the T_g reported for Ultem 1000,[8] at a rate of 20 °C/min. The sample was allowed to equilibrate for 5 min. Then the sample was cooled from 270 °C to 35 °C at 20 °C/min e. The samples were again allowed to equilibrate for 5 min. The samples were put through this cycle eight times, where the heating, cooling, and equilibration count as one complete cycle. The seventh cycle was used to determine T_g using Universal Analysis software (TA Instruments, New Castle, DE).

RTI

Thermogravimetric (TGA) analysis studies were conducted to determine the thermal degradation of behavior of membrane films made from the highly thermally stable polymers studied. Membrane samples were heated in an inert He environment and a syngas mixture atmosphere at 10 °C/min from room temperature to 800 °C in a TA Instruments TGA instrument (Model 2050; New Castle, DE). The dual-scan TGA protocol ultimately used for the thermal decomposition experiments allowed for residual solvent/moisture removal. TGA Scan #1 was done in *helium* by heating samples from room temperature to 250 °C, holding them at 250 °C for 30 min, and then cooling them to room temperature. Immediately following the cooling step in helium, TGA Scan #2 then heated the samples in *inert He or syngas* from room temperature to 800 °C and held them at this final temperature for 30 min for PBI-based membranes. The TGA Scan #2 for Ultem 1000 and PBO samples were heated from room temperature to 750 °C and held for 30 minutes. The membrane materials investigated in the TGA studies were (i) pure PBI and nanoparticle (SiO_2 or Ni)-filled PBI films, (ii) SiO_2-filled and –unfilled Ultem 1000 films provided by UT, and (iii) four SiO2-filled and –unfilled PBO films (also from UT). The 10-nm SiO_2 particle content in the Ultem 1000 films were 0, 5, 10, 15, and 20 vol%. The PBO-based membrane films were prepared through the thermal conversion of hydroxy-containing polyimides in the temperature range of 350–450 °C. The preparation conditions for the PBO-based membranes are presented in Table 5.

Table 5. Sample Preparation Conditions for the PBO-Based (Filled and Unfilled) Membranes

Sample Name	Starting Material	Preparation Temperature (°C)	Filler added
6FPBO 450	6FDA-APAF Polyimide	450	No filler
6FPBO 400	6FDA-APAF Polyimide	400	No filler
6FPBI_phil_Si(0.5)	6FPBO	400	0.5 wt% hydrophilic fumed silica
6FPBI_phil_Si(1.0)	6FPBO	400	1.0 wt% hydrophilic fumed silica

5. Results and Discussion

5.1. High-Temperature Membrane Films

UT

Ultem 1000 films, both unfilled and filled with MgO, SiO_2, or Cu nanoparticles, have been prepared using the solution-casting method. These films were approximately 200 μm thick, and were sufficiently robust to be cut, using scissors, into coupons that could subsequently be tested for pure gas

permeability. Once a film exhibited CO_2/light gas selectivity of 1 the nanoparticle was considered to have surpassed its maximum loading for practical usage for membranes applications and higher loadings of that nanoparticle in Ultem were not explored.

RTI

PBI membranes, both unfilled and filled with SiO_2 or catalytic Ni/Al_2O_3 nanoparticles, were prepared for permeation and thermal stability testing studies. Because the initial thin (6- to 8-µm-thick), unfilled Celazole PBI films made by knife-casting were found to have defects (i.e., pinholes) during permeation tests, thicker PBI films were formed by solution-casting into glass rings supported on glass plates. Though earlier thick PBI films had been too brittle and "wrinkly" (i.e., not flat) for permeation tests, we could now prepare more robust PBI membranes after several attempts at making them under various film casting and drying conditions. Pure PBI films were also prepared from an unspecified grade provided by Pall Corporation. Films were cast continuously throughout the project duration to tweak the knife-gap clearance and drying method to make defect-free PBI/nanocomposite films. The solution-cast PBI-based films were immediately placed in a 70 °C oven with N_2 purge to dry for 24 h and then post-heat-treated to ensure complete solvent and moisture removal.

A proper post-heat-treatment protocol for the cast membrane films was established with the help of TGA studies. TGA data indicated that only half of the leftover moisture/solvent was removed by post-heat-treating the PBI-based membranes at 250 °C for 18-20 h. For the pure PBI sample, the TGA Scan #1 weight loss was ~23% with no post-treatment and ~11% with 250 °C post-treatment. The Scan #1 weight loss was similar for the 10 wt% SiO_2/PBI nanocomposite: 21% and 10% without and with the 250 °C post-treatment, respectively. An important discovery was made through this analysis that high-temperature post-treatment did not affect the final decomposition temperature of the PBI-based membranes. The degradation onset temperature was ~566-567 °C and ~568-570 °C for the pure PBI and 10 wt% SiO_2/PBI blend samples, respectively, regardless of whether a post-treatment was done.

After TGA results showed the presence of measurable amounts of residual solvent and/or moisture in the PBI-based membranes dried at 250 °C for 24 h, a more aggressive post-heat treatment step was evaluated. The effectiveness of this post-heat treatment step was examined through TGA analysis. First, bulk drying of solvent-cast films occurred for 24 h in a 70 °C oven with N_2 purge. After the essentially dry films were removed from the glass casting surface, they were returned to the oven at 350 °C for another post-heat treatment under N_2. The time for the post-heat treatment was varied for times including 0.5, 1, and 24 h to find the shortest amount of time to remove an adequate amount of residual solvent and/or moisture.

TGA scans indicated that for the times evaluated, the 1-2 hours at 350 °C eliminated a sufficient amount of the residual solvent in minimal treatment time. Figure 4a displays the effect of post-heat treatment times at 350 °C on the residual TGA weight of the sample. Heating for 1 h is slightly different than heating for half an hour. A bigger difference was seen when the film is treated for 24 h, but the difference in residual weight percent is not substantial enough to justify using such a long treatment time.

Figure 4b illustrates the significant improvement in driving off the residual solvent and moisture from the membranes with the post-heat treatment protocol. This plot compares the TGA results obtained for Celazole PBI with no heat treatment (i.e., 70 °C drying) with 250 °C heat treatment for 18-20 h, and with 350 °C heat treatment for 24 h. While the difference between the no heat treatment and the post-heat treatment is significant, the difference between 250 and 350 °C treatments is minimal. In the end, the initial weight loss remaining after post-heat treatment may simply be the equilibrium sorption of ambient moisture (roughly ~10 wt%) into the PBI sample. Due to recently discovered limitations with the oven,

the post-heat treatment protocol has been finalized to be 300 °C for 2 h. Once installed in the permeation cell, the films will then be heated overnight at 100 °C before testing begins. This will allow any sorption of ambient moisture to be driven from the PBI membrane before testing.

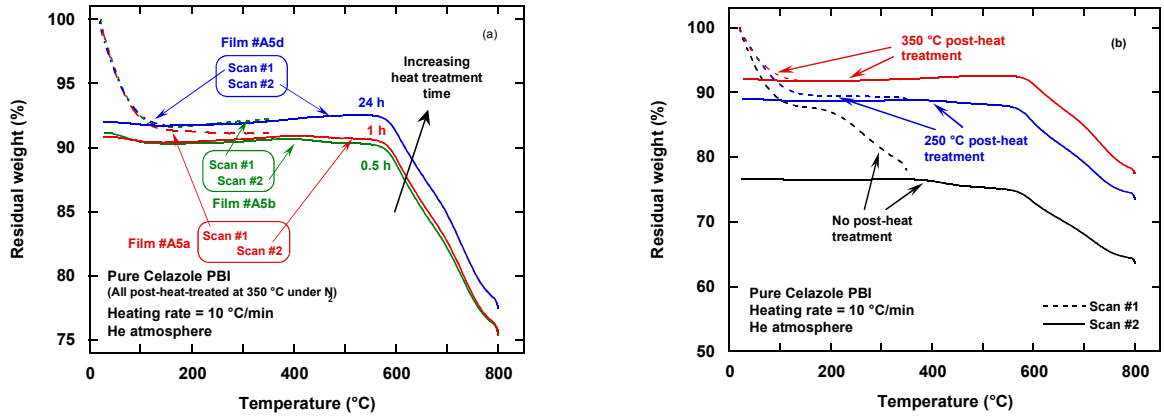

Figure 4. TGA scan weight loss profiles for (a) PBI resin post-heat-treatment times of 0.5 h, 1 h and 24 h at 350 °C and (b) PBI resin with no post-heat treatment and for post-heat treatment at the temperatures 250 °C (18-20 h) and 350 °C (24 h).

5.2. Pure- and Mixed-Gas Permeation Properties of Thermally Stable Polymer Membranes

5.2.1. Unfilled High-Temperature Polymer Membranes

UT

The preparation and gas transport properties of Ultem 1000 are reported in section 5.2.2. with nanoparticle filled Ultem.

RTI

Pure H_2 and CO_2 permeation properties of a 19-µm-thick Celazole PBI film (Sample #A1) and a 34-µm-thick Pall PBI film (Sample #B1) were measured at 23 °C over a feed pressure range of 100-300 psig. These data are presented in Table 6. Both PBI films have a pure H_2/CO_2 selectivity of 6-7 and very low permeability (1.2-1.7 barrer for pure H_2; 0.2-0.25 barrer for pure CO_2). Continued characterization of these two films at higher temperatures and/or with a syngas feed could not be done because they became defective upon further testing.

Pure H_2 and CO_2 permeation properties of a 21-µm-thick Celazole PBI film (Sample #A4) and a 35-µm-thick Pall PBI film (Sample #B2) were evaluated. Permeation properties for Sample #A4 measured at ~200psig over a temperature range of 23-250 °C could not be continued for a complete characterization of this film for CO_2 and/or with a syngas feed because the membrane became defective upon further testing. Sample #B2 was characterized over the temperature range of 23-250 °C at 200 psig. A complete study for these varying temperatures and with a syngas feed were determined. The PBI Sample #B2 has a pure H_2/CO_2 selectivity of approximately 13-16 over the specified temperature range. Comparisons of the permeabilities and selectivities for the pure and mixed gas analyses are presented in Figure 5. All permeabilities increase with increasing temperature. Comparison of the pure and mixed gas permeabilities for H_2 and CO_2 as well as the H_2/CO_2 selectivity showed negligible differences. The

H_2/CO selectivity decrease with increasing temperature can be explained by a greater increase in CO permeability relative to the H_2 permeation through the membrane.

Table 6. Pure H_2 and CO_2 Permeation Properties Measured for Dense PBI Film Samples #A1 and #B1 at 23 °C

PBI film	Feed pressure (psig)	Pure-gas permeability (barrer)		Pure H_2/CO_2 selectivity
		H_2	CO_2	
Sample #A1	100	1.2	—[a]	—
	201	1.2	0.20	6.0
	300	1.4	0.20[b]	7.0
Sample #B1	100	1.7	—[a]	—
	200	1.5	0.25	6.0
	304	1.4	0.20	7.0

Film thickness = 19 µm (Sample #A1); 34 µm (Sample #B1)

Permeate pressure = 0 psig; Downstream He sweep rate = 14-43 cm^3/min

[a] Too low to be measured (determined) on permeation system used.

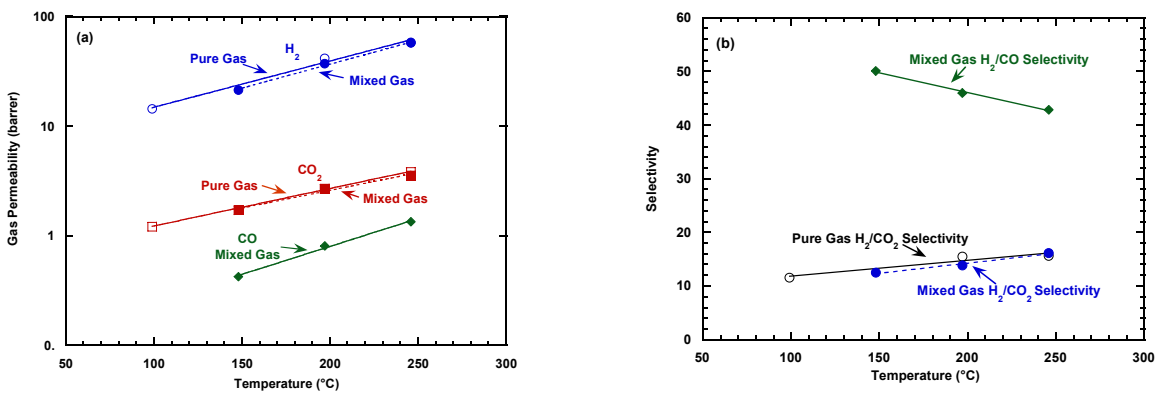

Figure 5. Effect of temperature on pure- and mixed-gas (a) syngas permeabilities and (b) H_2/CO_2 and H_2/CO selectivities for PBI Sample #B2. Process conditions included the pressure being held at 200 psig, while the temperature was varied from 100–250 °C. Mixture tests were performed with a ternary syngas (36.8% H_2, 12.5% CO_2, and 50.7% CO). Film thickness = 35 µm. Permeate pressure = 0 psig. Downstream He sweep rate = 20 cm^3/min.

Celazole PBI Sample #A5M was tested to obtain pure-gas and syngas mixture permeation properties at ~200 psig and 98 °C (Table 7). Continued characterization of this film at different temperatures could not be completed because the membrane became defective upon further testing. Two samples were cut from the host film A6, Samples #A6-1 and #A6-2M. Sample #A6-1 was characterized at 98 °C and 202 psig feed pressure using pure gases and the three-component syngas mixture (Table 7). Unfortunately, upon completion of this first set of tests, the film cracked in the permeation cell overnight. A thorough characterization for Sample #A6-2M was completed over the temperature range of 100-250 °C at 200 psig for pure H_2 and CO_2 and syngas feed. Comparisons of the pure- and mixed-gas

permeabilities and selectivities for Sample #A6-2M are presented in Figure 6. Sample #A6-2M exhibited a large variation between the CO_2 permeabilities of the pure and mixed gas.

Table 7. Permeability Data for PBI Membrane Samples #A5-M and #A6-1 at 98 °C

Sample	Gas	Permeability (barrer)			Selectivity	
		CO	H_2	CO_2	H_2/CO_2	H_2/CO
A5-M	Pure Gas					
	Pre-syngas	-	23	2.1	11	
	Post-syngas	-	17	2.2	7.7	
	Syngas Mixture[a]	2.54 [b]	13	3.7	3.5	5.03
A6-1	Pure Gas					
	Pre-syngas	-	9.8	0.8	12	
	Post-syngas	-	9.5	0.6	16	
	Syngas Mixture[a]	.3 [c]	10	3.1	3.2	33

A5-M film thickness = 13 µm; Masked film area = 2.8 cm^2

A6-1 film thickness = 30 µm

Feed pressure = 202 psig; Permeate pressure = 0 psig

Downstream He sweep rate = 20 cm^3/min

[a] Syngas mixture composition = CO_2 – 12.48%, H_2 – 36.78%, and CO - Balance

[b] CO permeability is unusually high, which could indicate developing defect in the film.

[c] Values computed using manually integrated GC peak for CO concentration.

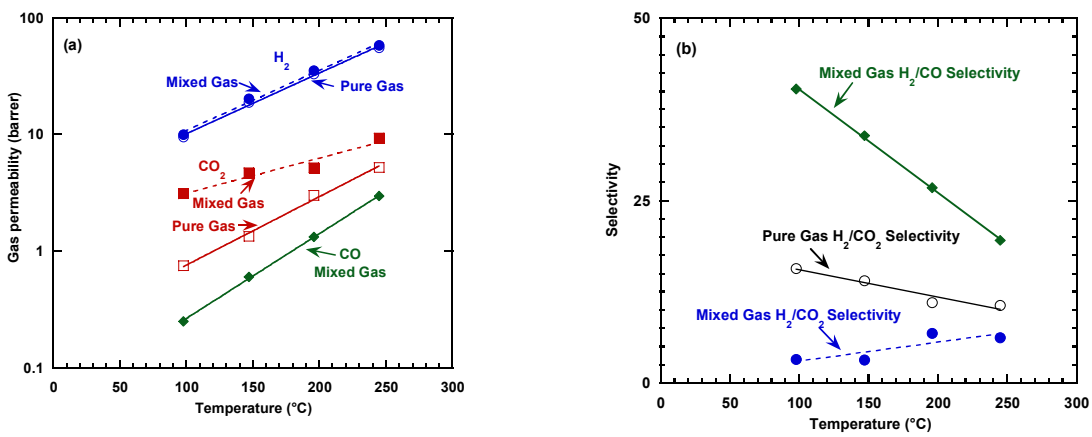

Figure 6. Effect of temperature on pure- and mixed-gas (a) permeabilities and (b) selectivities for PBI Sample #A6-2M. Process conditions included the pressure being held at 200 psig, while the temperature was varied from 100–250 °C. Mixture tests were performed with ternary syngas (36.8% H_2, 12.5% CO_2, and 50.7% CO). Film thickness = 30.4 µm; Masked area = 2.54 cm^2. Permeate pressure = 0 psig. Downstream He sweep rate = 20 cm^3/min.

The permeation properties of Sample #A6-2M are also compared to results obtained for PBI Sample #A4 in Figure 7 and PBI Sample #B2 in Figures 7 and 8. Pure H_2 permeability between PBI Samples #A4, #B2, and #A6-2M vary negligibly as observed in Figure 7a. Samples #B2 and #A6-2M

also varied only slightly in pure- and mixed-H_2 permeability values, therefore all H_2 permeation was virtually the same for these samples. As seen in Figure 6, PBI Sample #A6-2M exhibited an increase in permeability with increasing temperature. However, it is seen in Figure 7b that, unlike PBI Sample #B2, the pure- and mixed-gas CO_2 permeabilities were not close in value and seem to have a slope change from 150 to 200 °C. Figure 8 indicates that the pure-gas H_2/CO_2 selectivity also decreased in value with increasing temperature in contrast to PBI Sample #B2. Both the H_2/CO_2 and the H_2/CO selectivities were found to be greater in value for Sample #B2 than for Sample #A6-2M.

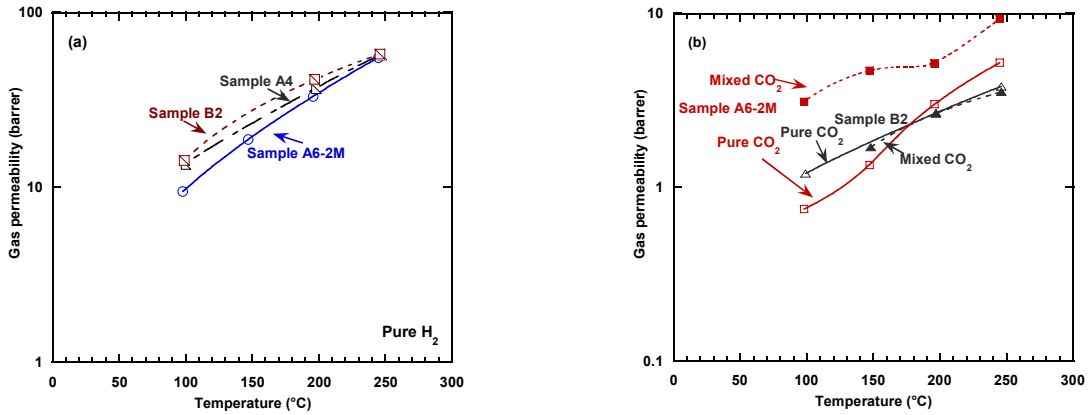

Figure 7. Effect of temperature on (a) pure H_2 permeability for Samples #B2, #A4, and #A6-2M and (b) pure and mixed CO_2 permeabilities for Samples #B2 and #A6-2M. Process conditions included the pressure being held at 200 psig while the temperature ranged from 100 – 250 °C. Mixture tests were performed with ternary syngas (36.8% H_2, 12.5% CO_2, and 50.7% CO). Permeate pressure = 0 psig. Downstream He sweep rate = 20 cm^3/min.

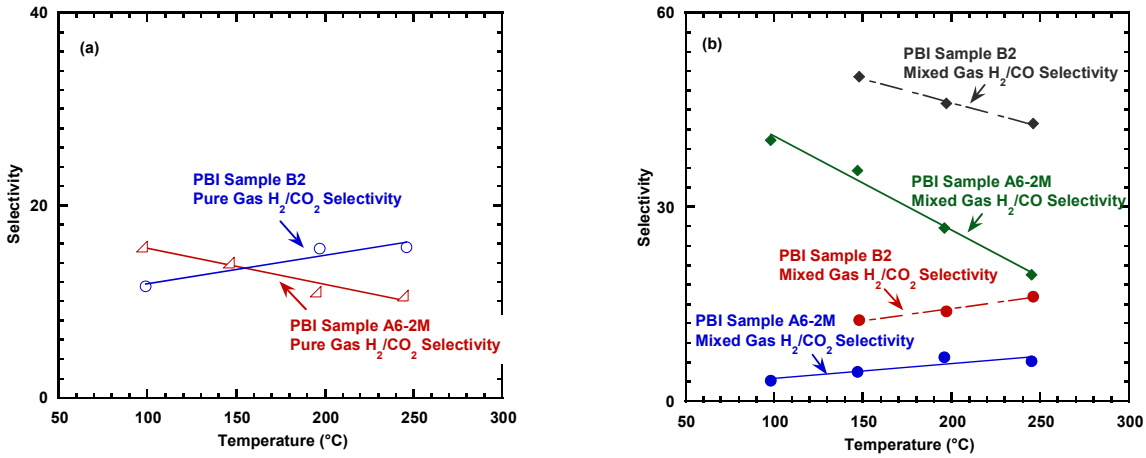

Figure 8. Effect of temperature on (a) pure-gas H_2/CO_2 selectivity and (b) mixed-gas H_2/CO_2 and H_2/CO selectivities for Samples #B2 and #A6-2M. Mixture tests were performed with ternary syngas (36.8% H_2, 12.5% CO_2, and 50.7% CO). Permeate pressure = 0 psig. Downstream He sweep rate = 20 cm^3/min.

5.2.2. High-Temperature Polymer Nanocomposite Membranes

UT

The nanoparticle filled Torlon AI-10 films became brittle and were prone to cracking before the drying step was complete. Fragility and the limited ability of the Torlon-based nanocomposites to form films appear to be independent of filler type. Due the fragility of the Torlon based materials, we were unable to prepare films that were appropriate for permeation experiments. Thus, the investigation of Torlon as a candidate polymer matrix material was discontinued.

Unless otherwise noted, methylene chloride was used as the solvent for Ultem 1000. Chloroform evaporated very quickly, which caused issues in pouring the nanoparticle filled polymer solution and in casting level films. Solutions prepared with methylene chloroform did not experience these issues.

SiO_2 disperses more uniformly in Ultem 1000 than MgO, as shown in Figures 9a and 9b. Even at higher loadings (i.e., 0.20 volume fraction SiO_2), the SiO_2 nanoparticles do not visually appear to form agglomerates, whereas agglomerates are visible in MgO-filled nanocomposites at lower loadings (i.e., 0.13 volume fraction MgO) [yellow arrows in Figure 9b]. Films of Ultem 1000 have been prepared with 0.05, 0.10, 0.15, and 0.20 volume fraction SiO_2. The particles are visually well dispersed in these films.

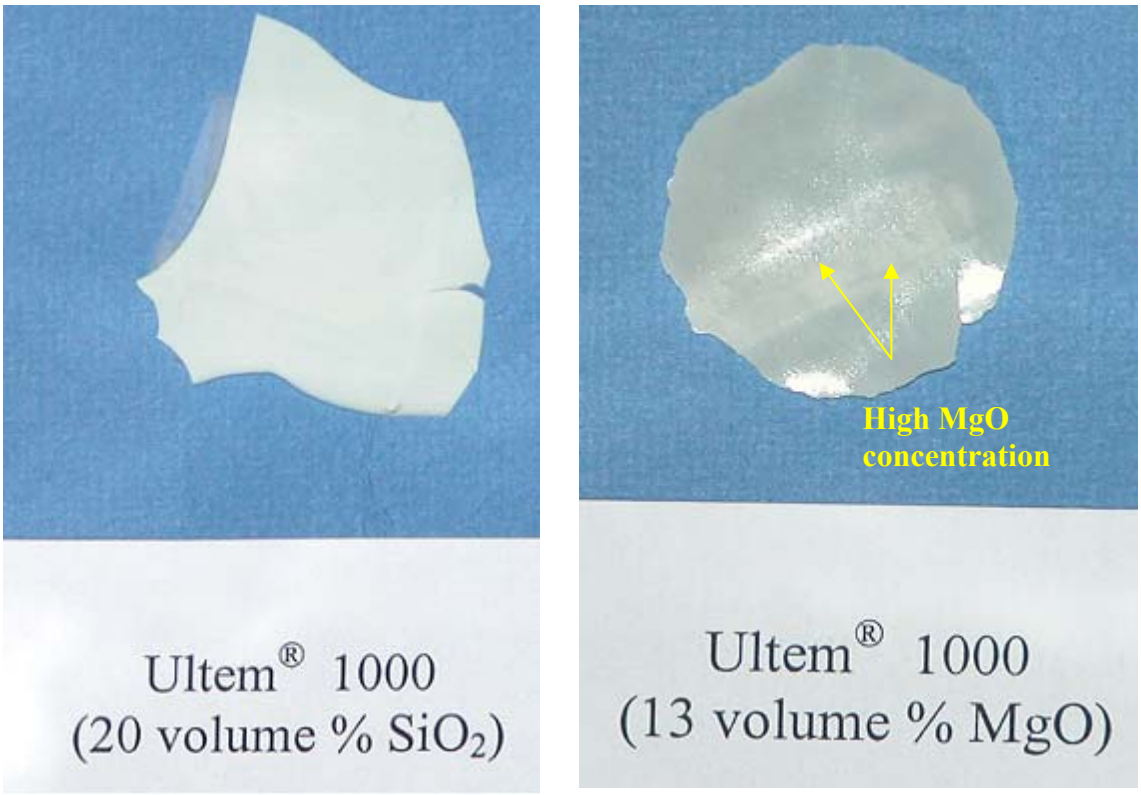

Figure 9. Photographs of Ultem 1000 filled with 0.20 volume fraction SiO2 nanoparticles of 10-nm primary particle diameter (a), and of Ultem 1000 filled with 0.13 volume fraction MgO nanoparticles of 3-nm primary particle diameter (b). Yellow arrows indicate regions of high nanoparticle concentration relative to majority of the nanocomposite.

Attempts have been made to make nickel filled Ultem 1000 nanocomposite films. The nanoparticles have not been uniformly dispersed within the composite. One issue has been the density differential between the nanoparticles and the polymer solution, which causes the nanoparticles to precipitate from solution during film casting if the polymer solution viscosity was sufficiently low. One remedy is to increase the polymer solution viscosity to impede nanoparticle precipitation. The viscosity is raised by increasing the ratio of polymer to solvent. Given the solvents used to date for Ultem 1000 (i.e., methylene chloride, chloroform), the solvent evaporates quickly, and causes a high viscosity (polymer rich) solution to dry before a film can be prepared, and often before the solution is even properly poured.

Another issue has been the mixing of the particles into solution. Since the Ni particles contain trace amounts of iron, it is not possible to use magnetic stirring rods to disperse the particles as the particles tend to agglomerate around the rod. Although ultrasonication has been able to break up agglomerates of nanoparticles, the particles are also able to sink to the bottom of the mixing vessel during the sonication process. Finally, the best results have been by vigorously shaking the mixing vessel by hand. Beyond other drawbacks, this method still leaves sizeable agglomerates of Ni in the resulting membranes. Another solution may be to mix the particles in solution using a blender. To date this method has not been attempted due to the sample size required for blending (>100 mL solution). Also, the current solvents may evaporate during mixing, which may cause difficulties in subsequent film casting.

Three samples of copper filled Ultem 1000 were prepared by dissolving 1.5 g of Ultem 1000 in 20 mL methylene chloride. Once the polymer was completely dissolved (generally requiring <less than 1 hour) copper nanoparticles were added to the solution. The nanoparticles were dispersed by ultrasonication for 15 minutes. Immediately after ultrasonication, the sample solutions were poured into clean, dry, level casting plates and covered to slow evaporation. Samples were allowed to cast until they were solvent free, which generally took under two days. The three films contained 0.04, 0.09, and 0.12 volume fraction copper nanoparticles (25, 40, and 50 weight percent copper nanoparticles, respectively). The 0.04 and 0.09 volume fraction films were defect free and their permeability properties were characterized. The 0.12 volume fraction film was not defect free.

Permeation results from the control, unfilled-Ultem, have been completed and the results are similar to the permeation values reported by Vu et al.,[8] as shown in Table 8. The difference in permeation values may have been caused by differences in sample preparation, (e.g., rate of evaporation, polymer concentration in solution, etc.).

Table 8. Permeation Data for Ultem 1000 Nanocomposites at 35 °C and $\Delta p = 3.4$ atm

Sample	Permeability [Penetrant size, Å][9] (barrer)				
	H_2 [2.89]	O_2 [3.46]	N_2 [3.64]	CH_4 [3.8]	CO_2 [3.3]
Ultem 1000 tested by Vu[8]	—	0.38	0.05	0.04	1.45
Ultem 1000 tested by UT	9.4	0.76	0.14	0.03	3.3
Ultem 1000 with 0.07 volume fraction MgO	16.9	2.5	0.74	0.62	6.0
Ultem 1000 with 0.20 volume fraction SiO_2	17.5	2.2	0.64	0.85	9.6

MgO and SiO_2 filled Ultem 1000 nanocomposite films were tested for pure CO_2, N_2, O_2, H_2, and CH_4 permeability. For both MgO- and SiO2 filled Ultem 1000 nanocomposite films, gas permeability is

substantially higher than the unfilled polymer as presented in Table 8. The extent of permeability enhancement appears to be related to the size of the penetrant molecules. The permeability of H_2, the smallest molecule for which we have comparable data, doubles and the permeability of CH_4, the largest penetrant molecule tested, is 15 to 20 times higher. The dependence of permeability enhancement on the penetrant size may indicate the size-sieving capability of the filled films is being reduced, compared to unfilled Ultem, by adding nanoparticles.

A nanocomposite film of Ultem 1000 containing 0.03 volume fraction Ni nanoparticles has been tested for gas transport properties, and the results are listed in Table 9. Please note that CO_2 permeability was below the resolution of the testing equipment.

Table 9. Permeability of Ultem and Ni filled Ultem at 35 ^oC and Δp = 3.4 atm.

Sample	Permeability [Penetrant size Å][9] (barrer)				
	H_2 [2.89]	O_2 [3.46]	N_2 [3.64]	CH_4 [3.8]	CO_2 [3.3]
Ultem 1000 tested at UT	9.4	0.76	0.14	0.03	3.3
Ultem 1000 filled with 0.03 volume fraction Ni	8.0	--	--	0.14	--

Copper filled Ultem 1000 nanocomposite permeability has been characterized for a series of nanoparticle loadings. The pure gas permeability for CO_2, H_2, and CH_4 for the Cu filled Ultem films are presented in Table 10. At low loadings it appears the copper nanoparticles cause an order of magnitude increase in permeability while only causing a 20% drop in CO_2/CH_4 pure gas selectivity. However, the CO_2/H_2 selectivity of the composite has been reduced to ~1. However, when 0.09 volume fraction Cu is dispersed in Ultem, the light gas permeability and the CO_2/CH_4 selectivity begin to decrease as compared to the film containing 0.04 volume fraction Cu.

Table 10. Permeation properties of Cu filled Ultem 1000 nanocomposites at 35 ^oC and Δp = 3.4 atm

Copper loading in Ultem 1000 (volume fraction)	CO_2 Permeability (barrer)	H_2 Permeability (barrer)	CH_4 permeability (barrer)
0	3.3	9.4	0.03
0.04	26.6	32.8	0.3
0.09	9.0	8.2	0.12
0.12	NA	NA	NA

Two PBI films supplied by RTI have been characterized for permeability. A third film was defective and could not be tested. The permeability of the two films as well as their composition are listed in Table 11.

Table 11. Permeation properties of Ni filled PBI nanocomposites at 35 ^{o}C and Δp = 3.4 atm.

Nickel loading in PBI (volume fraction)	CO_2 Permeability (barrer)	H_2 Permeability (barrer)
0	0.4	2.2
0.04	0.4	1.8

It is not clear if any Ni particles were present in the sections of film that were tested. Large agglomerates were visible in the Ni filled sample, but these sections were purposely avoided in preparing the sample for permeability experiments.

RTI

Celazole PBI nanocomposite membranes were successfully prepared using SiO_2 and catalytic Ni/Al_2O_3 nanoparticles. The PBI/10-nm SiO_2 particles and PBI/Ni catalyst nanoparticle films were tested to obtain pure-H_2 gas permeation properties at 200 psig and 100 °C. Characterization of these films could not be completed because the membranes were defective. Table 12 provides a list of the PBI nanocomposite membrane films tested, where the designation "AS#-M" is for the nanosilica filler and "AN#-#M" is for the Ni nanoparticles. No samples had visible defects when put into the test system. Samples AS2-M and AS3-M could not maintain pressure. Samples AS4-M and AS5-M both reached the desired feed pressure without problem, but upon measuring the H_2 composition through GC analysis, it was apparent that the films were defective. Sample AS5-M increased in H_2 composition by 20% per minute run, going towards 100% H_2. Sample AS4-M appeared defect-free as the initial run was ~1.3% H_2,; however, the composition continually increased each run over a 30 minute period. The two masked samples made from a single host film, AN1-1M and AN1-2M, showed similar results. Sample AN1-1M could not maintain a pressure in the system. Sample AN1-2M achieved and maintained the desired feed pressure, but the H_2 composition was immediately ~100% in the GC analysis. This indicated that, for samples AS4-M and AN1-2M, a defect was present, albeit smaller, than the other samples. Consequently, membrane reactor studies could not be performed because PBI nanocomposite membranes doped with catalytic nanoparticles active for water-gas-shift or hydrogenation did not stay defect-free long enough to warrant evaluation of their membrane reactor properties. Rather the water vapor permeability obtained at 150, 225, and 265 °C in an earlier study in unfilled PBI will be used to simulate a water-gas-shift membrane reactor process in which shift catalyst is packed outside the PBI membrane for the subsequent technical and economic analyses of a high-temperature membrane process for H_2 purification.

Table 12. SiO_2- and Ni-Doped PBI Nanocomposite Films Tested for Permeation Properties

PBI film sample no.	Feed pressure (psig)
AS2-M	Defective
AS3-M	Defective
AS4-M	202
AS5-M	203
AN1-1M	Defective
AN1-2M	200

Four highly thermally stable polybenzoxazole (PBO)-based membranes (filled and unfilled with SiO_2 nanoparticles) were developed through the thermal conversion of hydroxy-containing polyimides in the temperature range of 350–450 °C at UT. The PBO films were extremely brittle and hard to handle making cutting permeation samples difficult. All four samples had to be masked for permeation testing. The unfilled PBO film Sample #6FPBO_400 and the 0.5 wt%-SiO_2-filled PBO nanocomposite film Sample #FPBI_phil_Si(0.5) did not maintain a pressure in the cell, indicating defects. The unfilled PBO film Sample #FPBO_450 sample did hold the desired pressure of 200 psig, but, upon completion of the pure gas analysis for H_2 and CO_2, the selectivity was 1. For the 1 wt%-SiO_2-filled PBO nanocomposite membrane Sample #6FPBI_phil_Si(1.0), its permeation data at 30 °C are shown in Table 13. Upon heating the film to 250 °C to characterize the film at a high temperature, the film could no longer maintain feed pressure, indicating defect formation in the film.

Table 13. Permeability Data for PBO Nanocomposite Membrane Doped with 1 wt% SiO_2 [Sample #6FPBI_phil_Si(1.0)]

Gas	Pressure (psig)	Temperature (°C)	Permeability (barrer)	H_2/CO_2 selectivity
H_2	202	31	79.30	3.65
CO_2	200	29	21.75	

Film thickness = 35.7 µm; Masked Film Area = 2.69 cm^2

Permeate pressure = 0 psig; Downstream He sweep rate = 20 cm^3/min

5.2.3. Thin-Film Polymer Composite (Multilayered) Membranes

RTI

The "proof-of-concept"' PBI composite (multilayered) membrane cast on a Mott Corporation 316L stainless steel support with 0.5-µm pore size was evaluated for permeation properties. Thin PBI layers had been deposited onto the support substrate by knife-casting and manual coating/spreading of a PBI solution (14 wt% in DMAc). To test this multilayered PBI composite membrane, the permeation cell had to be changed to one that would hold the square support substrate. In the first trial of the PBI composite on SS support, large gas leaks were caused by not having a complete seal inside the cell.

Addition of a second graphite O-ring allowed the desired 200 psig feed pressure to be maintained in the cell, but H_2 testing with GC analysis still indicated large defects in the PBI coating. The defects were a result of the coarse microporosity of the steel substrate. Much finer support microporosity would be needed to obtain a defect-free selective PBI coating. Such a coating was eventually achieved on a tubular, AccuSep (stainless-steel)-supported PBI composite membrane modules acquired from Pall Corporation.

The first tubular, AccuSep-supported PBI composite membrane module was evaluated with pure H_2 and CO_2. The feed pressures used in the module permeation tests were 100, 200, and 300 psig. The module test temperature varied from 23 to 200 °C. The pure-gas H_2/CO_2 selectivity data collected for the PBI composite membrane module #1 are summarized in Table 14. The low H_2/CO_2 selectivity values of the module raised the concern that the module was defective. Upon completion of the testing, the module was post-heat-treated to 400 °C. This post-treatment step caused defective spots in the membrane to become visible macroscopically. The module was then pressurized with pure N_2 in a beaker of water and, in the regions with notable changes in appearance, the N_2 gas bubbled through at a high rate, confirming the presence of defects in PBI Module #1.

For AccuSep-supported PBI composite membrane module #2, its apparent selective PBI layer thickness was 0.65 µm and the effective membrane area was 28.4 cm^2 according to Pall Corporation. Both of these numbers were used to compute the gas permeabilities from the raw permeation data. PBI Module #2 was first evaluated at room temperature with pure H_2 and CO_2 as a function of a feed pressure from 50 to 300 psig in 50-psig feed pressure increments. Because the pure-gas permeabilities were very low and exhibited the good pure H_2/CO_2 selectivity, the PBI module was considered defect-free.

Table 14. Selectivity Values for Tubular PBI Composite Membrane Module #1 at Varying Temperatures and Pressures

Feed pressure (psig)	Temperature (°C)	H_2/CO_2 selectivity
100	23	2.31
200	23	2.87
300	23	3.29
100	97	2.41
200	97	2.81
300	97	3.62
114	198	3.79
214	198	3.70
300	198	4.53

Pure-gas and mixture syngas permeability and selectivity results for the tubular PBI Module #2 at 20 and 300 °C are presented in Figure 10. At room temperature, the mixture H_2/CO_2 selectivity of 3-4 is

lower than the ideal (pure-gas) value of 5.4-8.4 apparently due to the lower H_2 permeability and higher CO_2 permeability measured under syngas mixture conditions, while at 300 °C the pure and mixed gas permeabilities and pure and mixed gas H_2/CO_2 selectivity are negligibly different. Moreover, the 300 °C plots in Figures 10c and 10d are representative of the permeation trends observed over the temperature range of 100-250 °C; hence, the plots for these other temperatures have not been included (repeated) here.

For tubular PBI Module #2 at 100 °C the mixture H_2/CO selectivity displayed a strong dependence on feed pressure and decreases from ~50 at 100 psig to 34.5 at 300 psig. This reduction in selectivity was a result of the CO permeability increasing more quickly than the H_2 permeability with increasing feed pressure. In contrast, the H_2/CO_2 selectivity showed much less pressure dependence. The mixture H_2/CO_2 selectivity of 16-17 was a little lower than the ideal (pure-gas) selectivity value of roughly 18–20 mainly because the CO_2 permeability measured under syngas mixture conditions was a little higher than that obtained under a pure-gas environment. The H_2 permeability was approximately constant over the experimental pressure range, having essentially the same value (1.1-1.2 barrers) under pure-gas and syngas mixture test conditions. Compared to the 20 °C results, the selectivities relative to H_2 (i.e., H_2/CO and H_2/CO_2) are much higher at 100 °C. Hence, on the basis of these two sets of temperature data, raising temperature appears to improve the hydrogen separation properties of PBI.

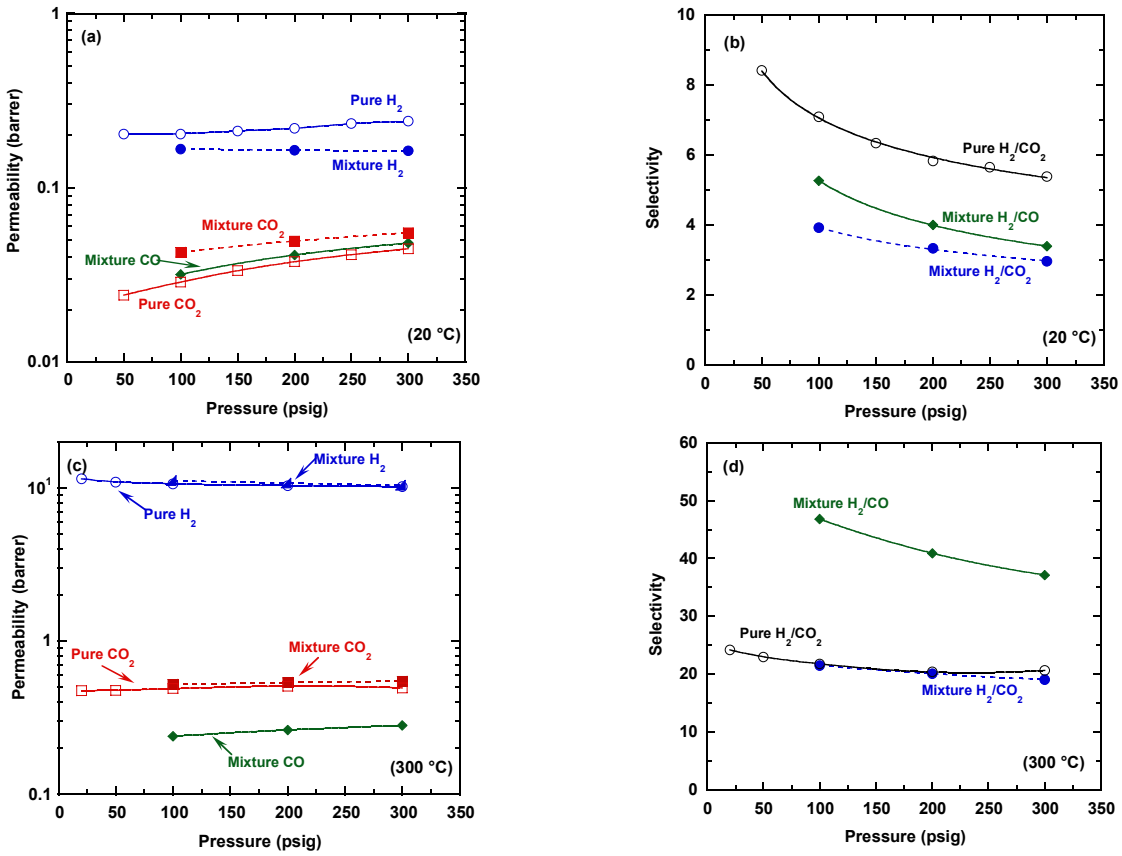

Figure 10. Effect of feed pressure on pure-gas and mixed-gas permeabilities and pure-gas and mixed-gas selectivities for tubular, AccuSep-supported, PBI membrane module #2 at (a) and (b) 20 °C and (c) and (d) 300 °C. Gas mixture used was a ternary syngas (36.8% H_2, 12.5% CO_2, and 50.7% CO). Permeate pressure = 0 psig; Downstream He sweep rate = 20 cm^3/min.

At 150 and 200 °C, the mixture H_2/CO selectivity values of PBI Module #2 were nearly the same over the experimental feed pressure range studied. The H_2/CO selectivity decreased from 71-74 at 100 psig to 60-62 at 300 psig. Pure- and mixed-gas selectivities and permeabilities obtained for PBI Module #2 at 250 and 300 °C were similar to those obtained at 150 and 200 °C; the mixture H_2/CO selectivity values of PBI Module #2 only varied somewhat for the two highest temperatures studied in this characterization. As previously reported, the H_2/CO selectivity values for 150 and 200 °C at 100 psig were ~71-74. As expected the H_2/CO selectivity values decreased from the previously measured selectivities to ~47-58 at 100 psig to ~37-52 at 300 psig. This showed that the pressure dependence of the H_2/CO selectivity appeared to be weaker at higher temperatures than at lower temperatures [i.e., observed selectivity reduction of 12-13 % at 250 °C and 15-16% at 150 and 200 °C versus 30-36% at 20 and 100 °C]. However, at an operating temperature of 300 °C, the observed selectivity reduction increased to 21-27%.

Relative to the H_2/CO selectivity, the H_2/CO_2 selectivity continued to exhibit consistently less dependence on feed pressure. For example, over the feed pressure range of 100-300 psig, the H_2/CO_2 selectivity is nearly constant at ~21-22 for 150 °C and ~22-25 for 200 °C. This trend continued at higher operating temperature yielding selectivity values of 22-24 and 19-21 for 250 and 300 °C, respectively. Although the selectivity values measured under pure- and mixed-gas conditions were very similar at the higher temperatures from 150 to 300 °C, the H_2/CO_2 selectivity usually tends to lie at the lower end of these selectivity ranges under mixed-gas conditions mainly because the mixture CO_2 permeability was somewhat higher than that obtained under pure-gas test conditions. The H_2 permeability stays essentially constant for the pure-gas and syngas mixture test conditions over the entire experimental pressure range for example 2.5-2.6 barrers at 150 °C; 4.4-4.6 barrers at 200 °C; 6.9-7.4 barrers at 250 °C; and 10.2-11.4 barrers at 300 °C.

Figure 11 illustrates the lack of pressure dependence of the PBI Module #2 permeability data for pure- and mixed-gas H_2 and CO_2 over the temperature range of 150 to 300 °C. At 100 °C, a slight variation between the mixed and pure gas permeabilities on the basis of component-gas feed partial pressure of the mixed gas was observed. Permeabilities do increase with increasing temperature as seen previously. At 20 °C, the difference was prominent. At 20 °C, the old permeation testing protocol for the module was being used. This entailed measuring H_2 then CO_2 properties at each pressure instead of completing the pressure characterization of H_2 before starting the CO_2 testing. Running the CO_2 at such a low temperature can induce plasticization effects that would have falsely increased the pure H_2 data. If plasticization occurred at this temperature during the mixed gas tests, this would also explain the unusually high CO permeabilities seen at 20 °C.

By plotting the permeability versus the mixed-gas feed-component partial pressure, the infinite-dilution, pure- and mixed-gas permeabilities (i.e., at zero partial pressure) were computed. Figure 12 displays the effect of temperature on the infinite-dilution, pure- and mixed-gas permeabilities for the thin-film PBI composite membrane module #2. Due to possible plasticization effects at 20 °C, this temperature point was omitted from both Figures 12 and 13 as it skewed the results from a linear fit.

Figure 13 presents an Arrhenius temperature dependence analysis of the permeability at three different feed pressures. Raising the temperature from 20 to 150 °C substantially improved module separation properties, leading to a 5- to 7-fold increase in H_2/CO_2 selectivity and a 15- to 20-fold increase in H_2/CO selectivity. This behavior could be attributed to the effects of the temperature on the diffusion and solubility selectivities. Since diffusion permeability was primarily controlled by size difference between the gas molecules, an increase in the polymer free volume allowed more gas to permeate. Here, as temperature increased, the polymer chains became more mobile, resulting in an increase in the free volume and allowing more small gas molecules such as H_2 to permeate. On the other hand, solubility permeability favors the larger, more condensable molecules like CO_2, which was not less affected by a

temperature increase. Despite the large increase in selectivity from room temperatures to 150 °C, raising the temperature from 100 to 150 °C illustrated that the H_2/CO_2 selectivity only increased by 16-30%, and the H_2/CO selectivity was just higher by 60%, relative to the 100 °C values. The thermal effect on the selectivity between 150 and 200 °C was slightly decreased in value, but at the time believed to be a negligible change. With the completion of the temperature dependence study, this minimal decrease in selectivity from 150 to 200 °C marked the start of a trend of decreasing selectivity with increasing temperature. This change in behavior indicated that, past a threshold temperature, the polymer chains are sufficiently mobile such that the size-selective versus solubility-selective permeation previously described was rendered void. This allowed for all measured gases to permeate freely, decreasing the selectivity seen previously (cf. May 2006 Report). This free volume increase can also explain the behavior of the observed H_2/CO selectivity reduction with increasing pressure at 300 °C. From 20 to 250 °C, observed selectivity reduction with increasing pressure decreased from 30-36% to 10-11%, then at 300 °C it increased to 20-27% by allowing more H_2 and CO through the polymer membrane. The pressure dependence of the H_2/CO selectivity increases because, with the degree that the free volume has increased at higher pressures, more gas is being pushed through the polymer membrane independent of the 'molecular sieve' diffusivity selectivity seen at lower temperatures. Utilizing the Arrhenius plots in Figure 13, the activation energies of permeation for the pure- and mixed-gas permeabilities were extracted and are reported in Table 15.

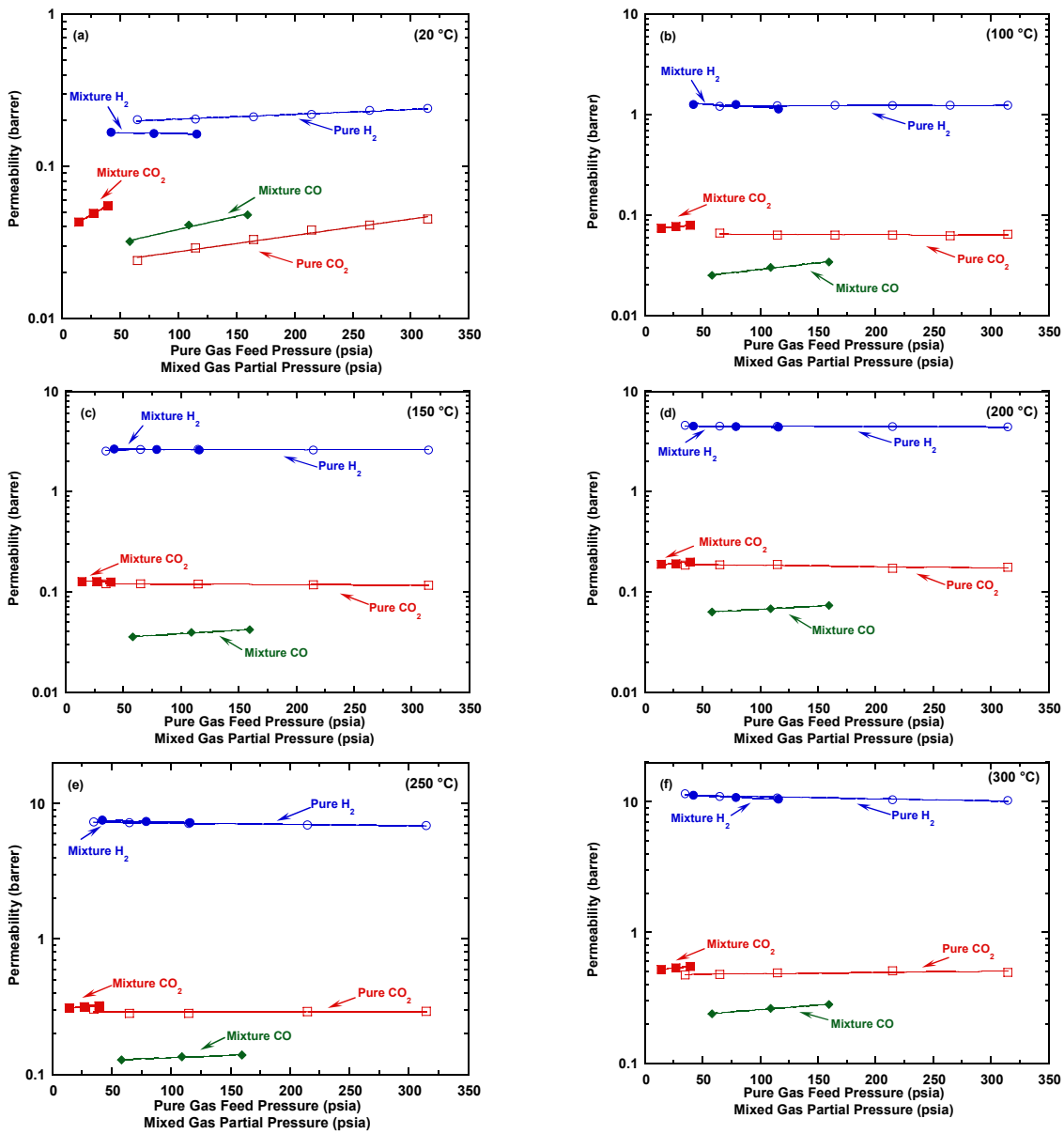

Figure 11. Comparison of mixed-gas and pure-gas permeabilities for tubular, AccuSep-supported, PBI membrane module #2 as a function of feed component-gas partial pressure at (a) 20 °C, (b) 100 °C, (c) 150 °C, (d) 200 °C, (e) 250 °C, and (d) 300 °C. Gas mixture used was the ternary syngas of 36.8% H_2, 12.5% CO_2, and 50.7% CO. Permeate pressure = 0 psig; Downstream He sweep rate = 20 cm^3/min.

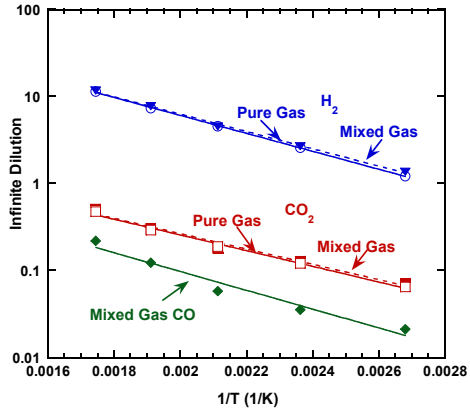

Figure 12. Effect of temperature on infinite-dilution pure- and mixed-gas permeabilities (expressed in barrer) of PBI composite membrane module #2. Process conditions included feed pressure being increased from 100 to 300 psig, while the temperature was varied from 100–300 °C. Gas mixture used was the ternary syngas of 36.8% H_2, 12.5% CO_2, and 50.7% CO.

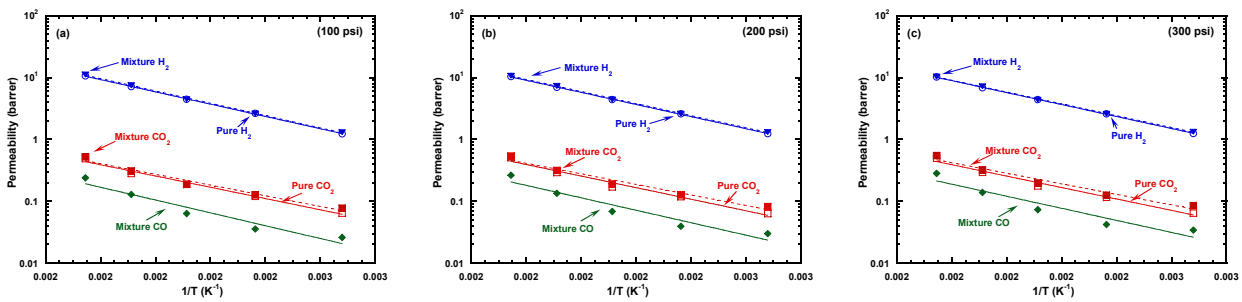

Figure 13. Arrhenius plots of pure- and mixed-gas permeabilities for tubular, AccuSep-supported, PBI membrane module #2 at feed pressures of (a) 100 psig, (b) 200 psig, (c) 300 psig. Gas mixture used was the ternary syngas of 36.8% H_2, 12.5% CO_2, and 50.7% CO. Permeate pressure = 0 psig; Downstream He sweep rate = 20 cm^3/min.

Table 15. Activation Energies of Permeation for Tubular PBI Composite Membrane Module #2

Feed pressure (psig)	Activation Energy (kJ/mol)				
	Pure Gas		Mixed Gas		
	H_2	CO_2	H_2	CO	CO_2
100	571.3	17.0	601.9	12.4	14.6
200	524.7	19.0	534.0	11.7	14.1
300	494.6	18.0	483.3	10.8	14.4

Upon completion of its entire temperature and pressure characterization, the PBI composite membrane module #2 was cooled back to 20 °C. The pure-gas permeabilities were remeasured at different pressures. At 20 °C, it was apparent that the pure-gas permeability had changed considerably. It was contributed to possible plasticization from using the old protocol of running both gases at each pressure before proceeding to the next pressure point. Therefore, the pressure characterization at 20 °C was redone utilizing the new protocol of running the entire pressure range with each gas before increasing

the pressure. Figure 14 shows the difference in permeabilities and selectivities between the new protocol and old protocol characterization. Due to this large variation at 20 °, Module #2 was reheated to 200 °C and retested with the pure gases at 100 psig feed pressure. The permeability and selectivity values at this point were unchanged, illustrating the presence of a temperature conditioning effect on the PBI membrane.

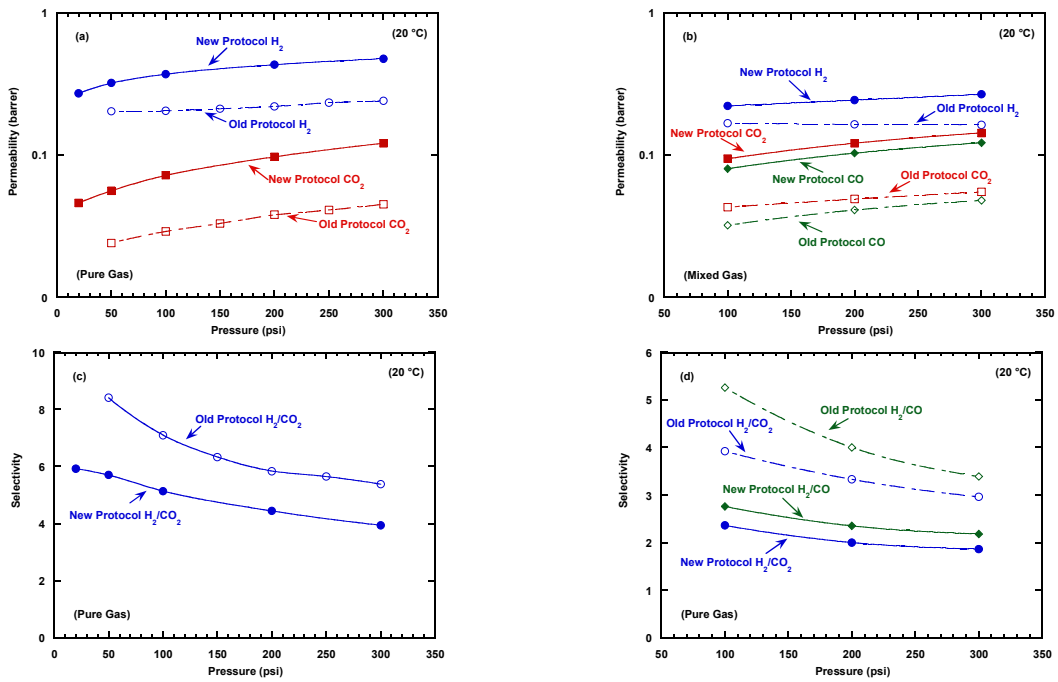

Figure 14. Effect of new and old testing protocols on pure- and mixed-gas permeabilities and selectivities at 20 °C for tubular, AccuSep-supported, PBI membrane module #2: (a) pure gas permeability; (b) mixed gas permeability; (c) pure gas selectivity; and (d) mixed gas selectivity. Gas mixture used was the ternary syngas of 36.8% H_2, 12.5% CO_2, and 50.7% CO. Permeate pressure = 0 psig; Downstream He sweep rate = 20 cm^3/min.

At 200 psig, the pure- and mixed-gas selectivities of the tubular PBI composite membrane module #2 data are compared in Figure 15 to those measured for the dense, free-standing PBI film Sample #B2. Both membrane film and composite membrane module display similar trends in selectivity from 100 to 200 °C. At 250 °C, however, the module H_2/CO_2 selectivity tends to decrease slightly for pure- and mixed-gas conditions.

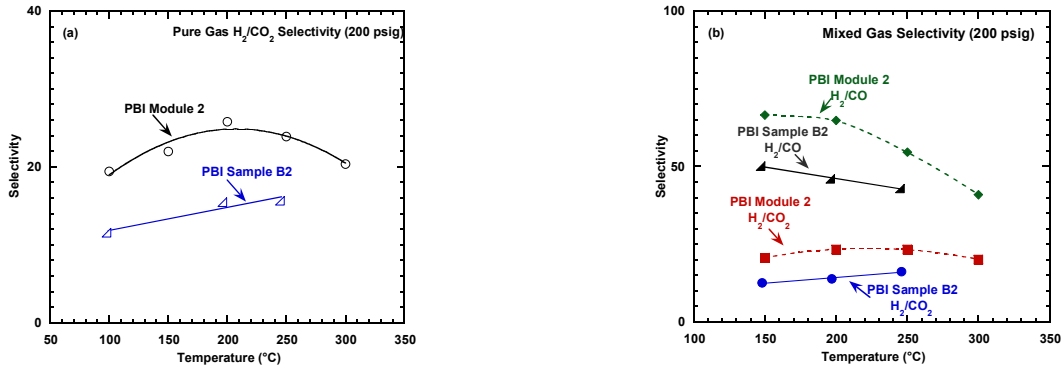

Figure 15. Comparison of the pure and mixture H_2/CO_2 selectivities and the mixture H_2/CO selectivity for the free-standing PBI film sample #B2 and PBI composite membrane module #2: (a) pure gas data and (b) mixed gas data. Process conditions are included in previous figure descriptions for the two samples. Gas mixture used was ternary syngas of 36.8% H_2, 12.5% CO_2, and 50.7% CO.

Upon completion of the comprehensive characterization of the gas permeation properties of tubular PBI composite membrane module #2, a four-component, H_2S containing syngas mixture was used to evaluate the membrane module from 100 to 300 psig at 300 °C. After the 100 psig test, pure H_2 and CO_2 were checked to ensure the H_2S had not adversely affected the membrane module, and then, post-pure-gas checks were also completed after the full pressure characterization was finished. Figure 16 presents a selectivity and permeability comparison of the H_2S-containing syngas mixture to both the pure gases and 3-component, no-H_2S syngas mixture. Figure 17 shows the feed component partial pressure comparison between the H_2S-containing and no-H_2S-containing syngas. No H_2S permeation through PBI composite membrane module #2 was observed until 300 psig. The H_2/H_2S and CO_2/H_2S selectivities were calculated to be 80 and 4.3, respectively.

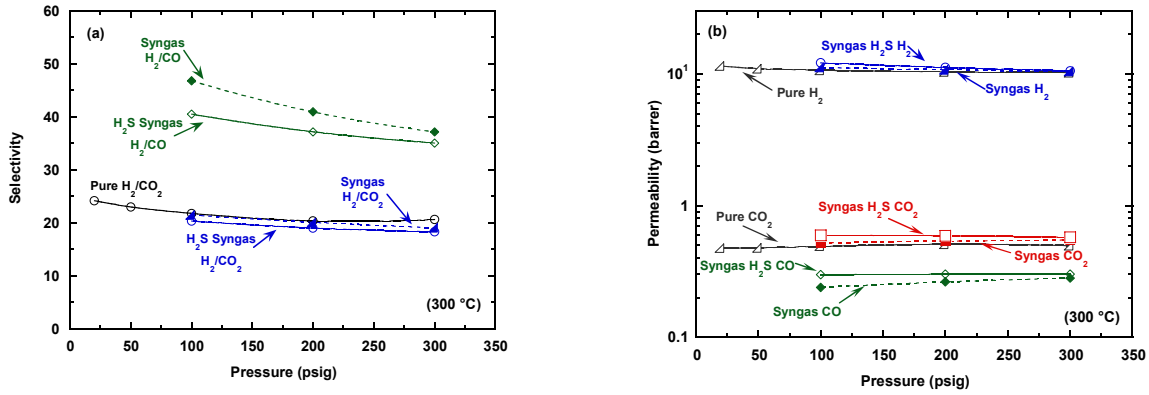

Figure 16. Comparison of permeation properties for PBI membrane module #2 at 300 °C evaluating (a) selectivity and (b) permeability with pure gases as well as H_2S-containing syngas and no-H_2S-containing syngas. Selectivities were computed from permeability data shown in (b). Mixture tests were performed with ternary syngas of 36.8% H_2, 12.5% CO_2, and 50.7% CO and 4-component syngas of 1.02% H_2S, 35.9% H_2, 13% CO_2, and 50.08% CO.

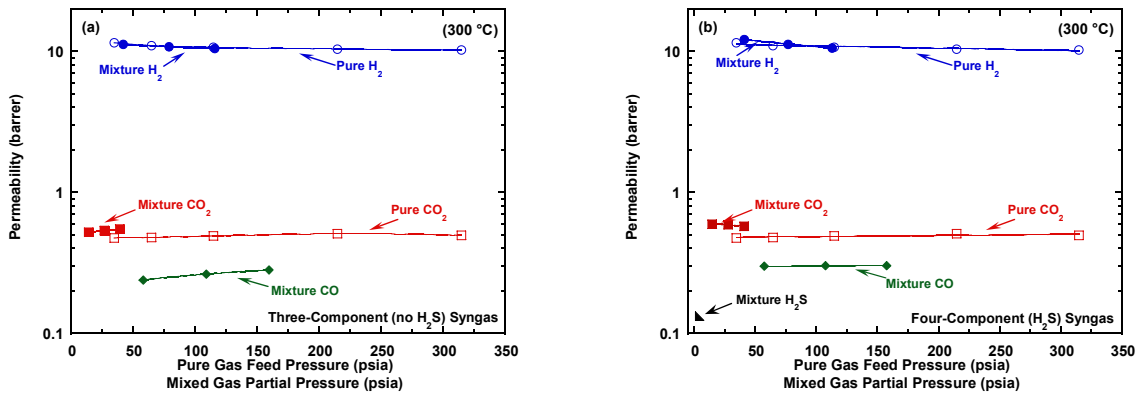

Figure 17. Feed component partial pressure plots for PBI membrane module #2 at 300 °C evaluating (a) no-H_2S-containing syngas and (b) H_2S-containing syngas. Mixture tests were performed with ternary syngas of 36.8% H_2, 12.5% CO_2, and 50.7% CO and 4-component syngas of 1.02% H_2S, 35.9% H_2, 13% CO_2, and 50.08% CO.

5.3. Thermal Properties of High-Temperature Polymer and Polymer Nanocomposite Membranes

UT

Ultem 1000 samples filled with SiO_2 nanoparticles have been studied using DSC. The data collected for Ultem filled with 0.05 volume fraction SiO_2 nanoparticles are shown in Figure 18 as an example. The unfilled Ultem 1000 had a T_g at 210 °C which is similar to the T_g report in the literature (i.e., 209 °C).[8] Addition of SiO_2 nanoparticles increased the T_g by 10 °C, even at loadings as low as 5 volume fraction SiO_2 as presented in Figure 19. The nanocomposite T_g gradually decreased from 220 °C with nanoparticle loadings in excess of 0.05 volume fraction SiO_2.

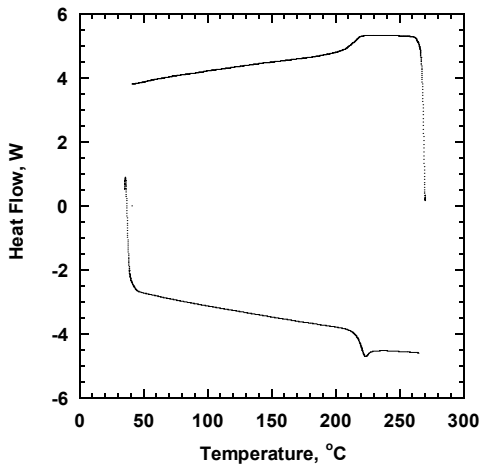

Figure 18. DSC of Ultem 1000 filled with 0.05 volume fraction SiO_2 nanoparticles.

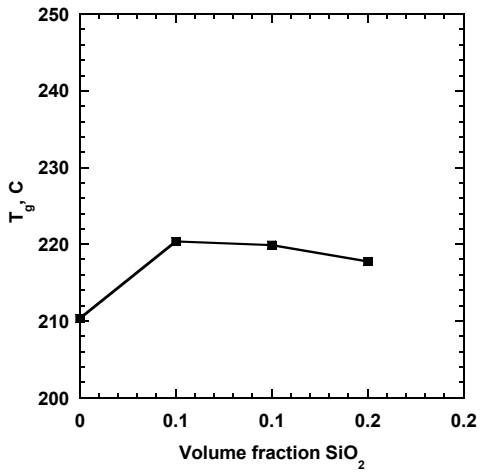

Figure 19. Glass transition temperatures for Ultem 1000 filled with increasing loadings of SiO_2 nanoparticles.

RTI

Unfilled Pall Corporation PBI and unfilled Celazole PBI were evaluated for differences in thermal stability in both a syngas and an inert He environment, as shown in Figure 20. The Celazole grade decomposition temperature (T_d) in He was around 566 °C, while the Pall grade had a higher T_d in He of 581 °C. In syngas, the T_d of the Pall PBI decreased to 566°C, and the Celazole PBI remained slightly lower at 558 °C. Though this short-term syngas exposure did tend to reduce polymer thermal stability slightly, the T_d was still much higher than the target operating temperature.

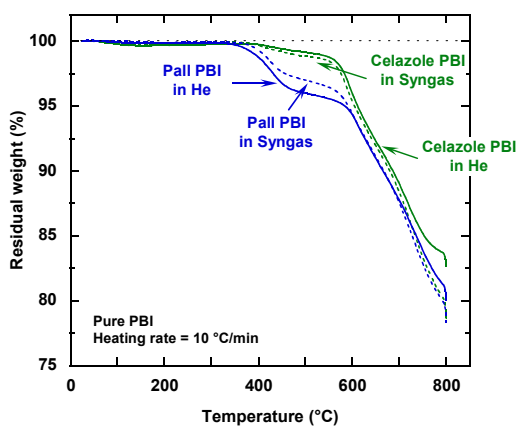

Figure 20. Comparison of TGA weight loss profiles in syngas and inert helium atmospheres for pure films of (a) Pall Corporation PBI and (b) Celazole PBI. All TGA scans were done at a 10 °C/min heating rate. Syngas composition used: 38.4% H_2, 14.8% CO_2, and balance CO.

A comparison of the thermal stability behavior of pure PBI, pure Ultem 1000 PEI, and pure PBO is made in Figure 21. It appeared that PBO made by thermal transformation at 450 °C (T_d ~ 500 °C in syngas) was a slightly more thermally stable than that transformed at 400 °C (T_d ~ 585 °C in syngas).

The PBI (T_d ~ 558 °C in syngas) exhibited a higher decomposition onset temperature than Ultem 1000 (T_d ~ 502 °C in syngas) and both PBO samples.

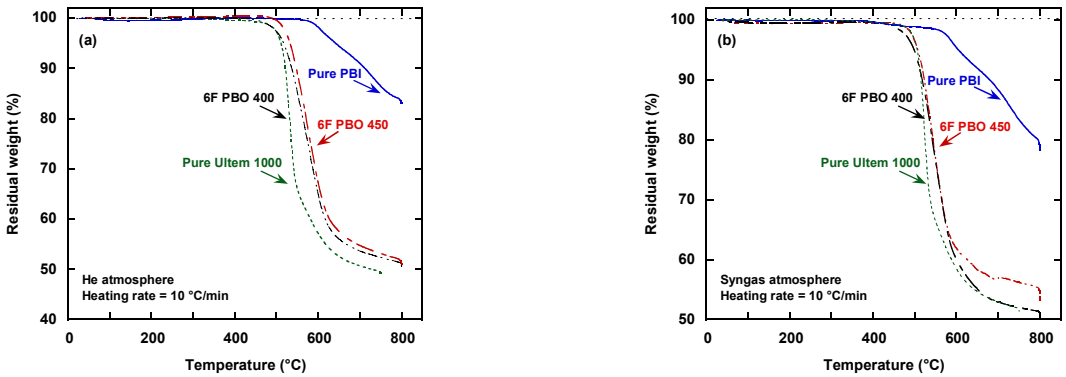

Figure 21. TGA curves for pure PBI, pure Ultem 1000 poly(etherimide) [PEI], and pure PBO in (a) helium environment and (b) syngas mixture environment. Samples were heated at 10 °C/min rate from room temperature to 800 °C for PBI samples and 750 °C for Ultem and PBO samples. Syngas composition used: 38.4% H_2, 14.8% CO_2, and balance CO.

The thermal stability results for the Celazole PBI/nanocomposites are compared to pure Celazole in Table 16. The first samples analyzed in an inert environment were not post-heat-treated to remove residual solvent and moisture. This post-heat-treatment step was added to the film drying protocol, and TGA was reanalyzed in He before going on to syngas analysis to ensure an accurate comparison of the two environments.

In helium, the decomposition temperature (T_d) of the PBI/10 wt% silica nanocomposite is ~567 °C, essentially unchanged from that of the unfilled, pure PBI. The decomposition temperature (T_d) of Celazole PBI in helium was 565/567 °C, while the 4.76 wt% Ni + Celazole PBI had a T_d of 570 °C showing that the addition of these nanoparticles neither enhance nor hurt the thermal stability of the PBI. In syngas, however, addition of 10 wt% SiO_2 and 4.76 wt% Ni catalyst does have a positive effect on the thermal stability of PBI. The PBI/10 wt% silica (T_d ~ 568 °C) and PBI/4.76 wt% Ni nanocomposites (T_d ~ 570 °C) are more thermally stable than unfilled PBI, whose T_d decreases from ~567 °C in helium to 558 °C in syngas. Figures 22 and 23 directly compare the TGA weight loss profiles in syngas and helium for the PBI/silica and PBI/Ni blends to the pure PBI, respectively, to illustrate how similar the decomposition onset temperature are in these two environments. The figures also indicate that thermal stability of the PBI/nanoparticle nanocomposites stays essentially the same regardless of whether the thermal degradation environment is in syngas or inert helium.

Table 16. Decomposition Onset Temperatures in Syngas and Inert Helium Atmospheres for Pure PBI and PBI/Nanoparticle Blend Nanocomposites

Sample	Decomposition onset T_d[b] (°C)	
	In syngas[c]	In helium
Pure PBI Resin		
Initial PBI Resin[a]	—	575
Post-heat-treated PBI Resin	558	565-567
Literature Data	-	600[g]
Celazole + 10 wt% SiO_2		
Initial PBI/SiO_2[a]	—	572
Post-heat-treated PBI/SiO_2	568	567
Celazole[a] + 10 wt% TS-530[d]	—	575
Celazole[a] + 30 wt% SiO_2[d]	—	572
Celazole + 4.76 wt% Ni/Al_2O_3	570	570

[a] Data was obtained before post-heat-treatment was added to film making protocol.

[b] Determined by TGA at 10 °C/min heating rate.

[c] Ternary syngas composition: 38.4% H_2, 14.8% CO_2, Balance CO.

[d] SiO_2 ≡ Hygroscopic, untreated, 10-nm silica nanopowder from Aldrich.

[e] TS-530 ≡ Treated Cab-O-Sil fumed silica with nonpolar trimethylsilylated [—$Si(CH_3)_3$] surface groups and 13-nm primary particle diameter.

[f] Ni/Al_2O_3 ≡ Ni catalyst nanoparticle made at RTI.

[g] Welsh, W. J., "Poly(benzimidazole)", In *Polymer Data Handbook*, Mark, J. E., Ed., Oxford University Press: New York, 1999, pp 288-290.

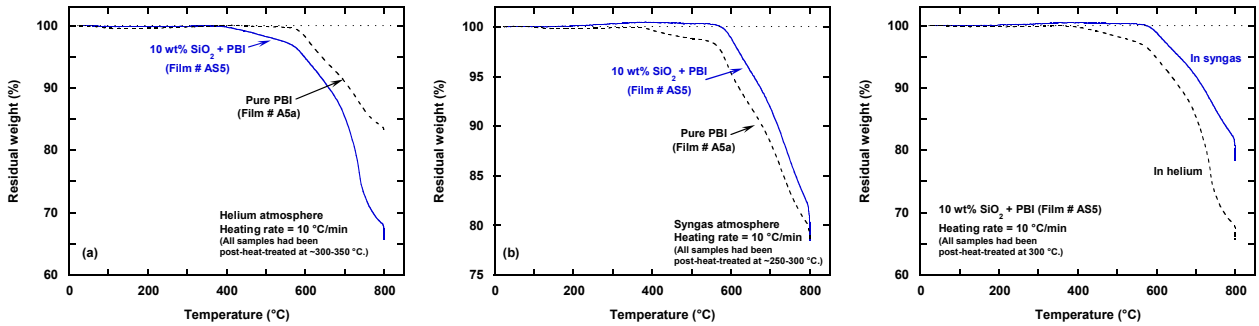

Figure 22. Comparison of TGA weight loss curves obtained for pure Celazole PBI and 10 wt% SiO_2/PBI nanocomposite blend in (a) inert He and (b) syngas and (c) for the nanocomposite film 10 wt% SiO_2/PBI in inert helium and syngas environments. All TGA scans were done

at a 10 °C/min heating rate. Syngas composition used was 38.4% H_2, 14.8% CO_2 and balance CO.

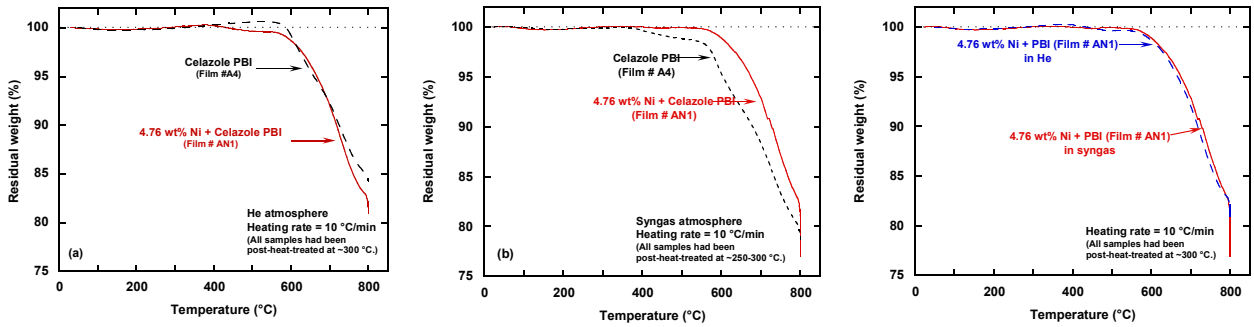

Figure 23. Comparison of TGA weight loss curves obtained for pure Celazole PBI and 4.76 wt% Ni/PBI nanocomposite blend in (a) inert He and)b) syngas and (c) for the nanocomposite film 4.76 wt% Ni Catalyst 041205a + PBI in inert helium and syngas environments. Syngas composition used was 38.4% H_2, 14.8% CO_2, and balance CO. TGA heating rate = 10 °C/min.

Figure 24 compares the TGA studies on PBI nanocomposite samples containing Ni and SiO_2 nanoparticles in a syngas environment. The 4.76 wt% Ni/PBI and 10 wt% SiO_2 nanocomposites showed a little more thermal stability than pure (unfilled) PBI sample, as indicated by rapid sample weight loss starting at higher temperatures. For all samples shown in Figure 24, the thermal decomposition temperature is 560 °C or higher, which is more than adequate for the high-temperature separation application targeted in this project.

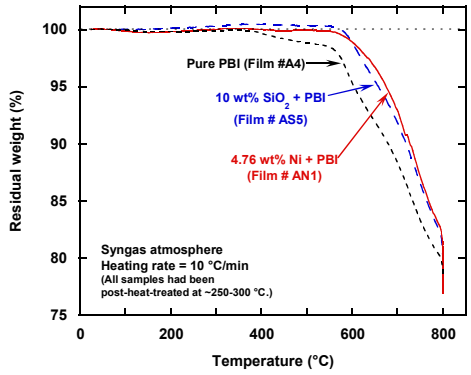

Figure 24. TGA weight loss curves obtained in syngas for pure PBI and PBI nanocomposite films doped with 4.76 wt% Ni catalyst (RTI Ni Sample #041205a-NiHRP) and 10 wt% SiO_2. TGA heating rate = 10 °C/min.

The TGA results for pure Ultem 1000 and the Ultem 1000/silica nanocomposites in the He and syngas environments are plotted in Figure 25 and Table 17. Relative to that for pure Ultem, the point of rapid thermal degradation for the SiO_2-filled Ultem nanocomposites is shifted slightly to the right toward higher temperatures. As a result, the decomposition onset temperature is a little higher for the Ultem/SiO_2 nanocomposites (~506-508 °C) than for pure Ultem (~502 °C). Closer analysis of the data shows that the decomposition temperature for Ultem and its nanocomposite blends with silica is about 8-13 °C lower in syngas than in helium. Though small, this temperature difference indicates that Ultem-derived films are slightly less thermally stable in a reducing gas environment. As a final observation, the final residue

weight at 750 °C increases with increasing silica content in Ultem. Therefore, the thermal stability of Ultem is improved slightly by addition of inorganic silica particles.

Figure 25. (a) Single-scan TGA weight loss profiles for Ultem 1000 PEI nanocomposites containing different loadings of Aldrich 10-nm SiO_2 nanoparticles in helium atmosphere. (b) Dual Scan TGA weight loss curves for Ultem 1000 PEI nanocomposites doped with Aldrich 10-nm SiO_2 nanoparticles in syngas environment of 38.4% H_2, 14.8% CO_2, and balance CO. In all tests, TGA samples were heated at 10 °C/min from room temperature to 750 °C.

Table 17. Comparison of Decomposition Onset Temperatures Measured in Syngas and Inert Helium Atmospheres for Pure Ultem 1000 PEI and SiO_2/Ultem 1000 PEI Blend Nanocomposites

Sample	Decomposition onset T_d[a] (°C)	
	In syngas[b]	In helium
Pure Ultem 1000 PEI		
This study	502	510
Literature data	—[d]	550[e]
5 vol% SiO_2[c] + Ultem 1000	506	519
10 vol% SiO_2[c] + Ultem 1000	508	519
15 vol% SiO_2[c] + Ultem 1000	507	518
20 vol% SiO_2[c] + Ultem 1000	507	519

[a] Determined by TGA at 10 °C/min heating rate.
[b] Ternary syngas composition: 38.4% H_2, 14.8% CO_2, Balance CO.
[c] Hygroscopic, untreated, 10-nm silica nanopowder from Aldrich.
[d] Not available in the literature.
[e] For an unspecified grade of PEI from Sepe, M. P., *Thermal Analysis of Polymers*, Rapra Review Report 95, Rapra Technology Ltd.: Shrewsbury, UK, 1997, Vol. 8, No. 11, p 17.

The PBO-based membranes were analyzed by TGA in a syngas environment and compared with TGA scans completed in an inert environment in Figure 26. Table 18 summarizes the decomposition temperature data obtained from the TGA analyses. In comparing the He and syngas TGA scans, short-term syngas exposure does tend to reduce polymer thermal stability slightly for all four samples. PBO made by thermal transformation at 450 °C is slightly more thermally stable than that transformed at 400 °C. Typically, addition of filler improves thermal stability. For He, adding 0.5% SiO_2 to the 400 °C-transformed PBO raises decomposition temperature by 5 °C. Upon adding 1% SiO_2, however, the decomposition temperature decreased by 9-10 °C. In syngas, the addition of SiO_2 to the 400 °C-

transformed PBO raises decomposition temperature by ~13 °C, which is a slightly more substantial increase than in the inert atmosphere. Upon adding 1% SiO_2, however, the decomposition temperature decreased significantly by ~19 °C. At this time, it is unclear why this would occur.

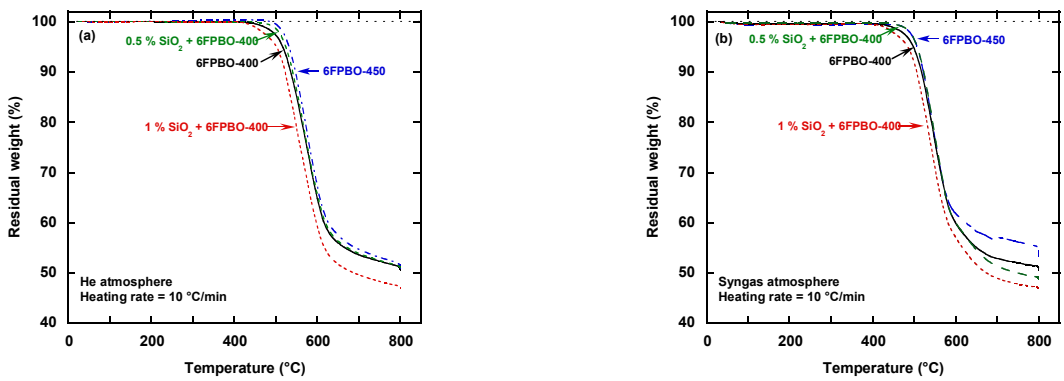

Figure 26. TGA weight loss curves for PBO nanocomposites. Samples were heated in (a) an inert He atmosphere and (b) a ternary syngas atmosphere at 10 °C/min from room temperature to 750 °C. Syngas mixture composition used was 38.4% H_2, 14.8% CO_2, and balance CO.

Table 18. Comparison of Decomposition Onset Temperatures Measured in Inert Helium and Syngas Atmospheres for Thermally Converted PBO and PBO Nanocomposite Samples

Sample name	Decomposition onset temperature (°C)	
	In syngas	In He
6FPBO 450	500	510
6FPBO 400	485	520
6FPBO_phil_Si(0.5)	498	515
6FPBO_phil_Si(1.0)	466	500

[a] Determined by TGA at 10 °C/min heating rate.
[b] Ternary syngas composition: 38.4% H_2, 14.8% CO_2, Balance CO.

Figure 27 provides a direct comparison of PBI, Ultem 1000, and PBO nanocomposites doped with SiO_2 in an inert He atmosphere as well as a syngas environment. The effect of silica particle addition on thermal stability of the host polymer is clearer for Ultem than for PBI or PBO. However, thermal decomposition values show that the PBI/SiO_2 nanocomposite (T_d ~ 568 °C in syngas) is much higher than that of the Ultem/SiO_2 nanocomposite (T_d ~ 508 °C in syngas) and PBO/SiO_2 nanocomposite (T_d ~ 466 °C in syngas).

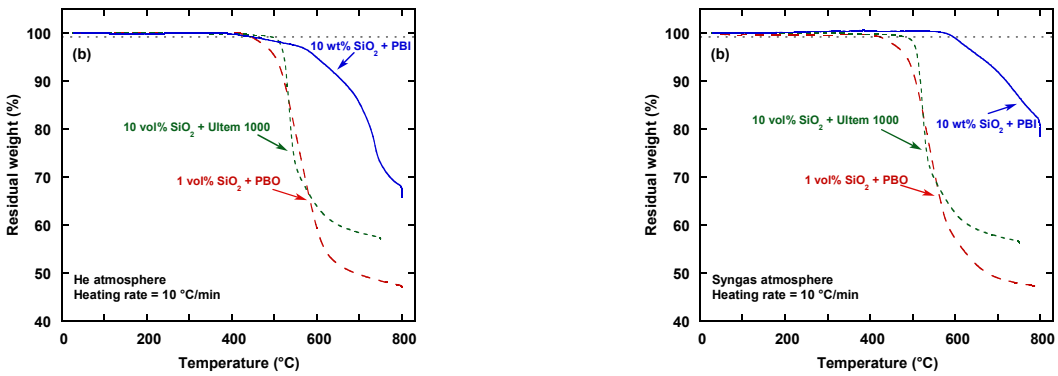

Figure 27. Comparison of TGA weight loss profiles for PBI/SiO_2 nanocomposite, Ultem 1000 PEI/SiO_2 nanocomposites, and PBO/SiO_2 nanocomposite in (a) He and (b) syngas. Samples were heated in an inert atmosphere at 10 °C/min from room temperature to 800 °C for PBI samples and 750 °C for Ultem and PBO samples. Syngas composition used: 38.4% H_2, 14.8% CO_2, and balance CO.

5.4. Technical/Economic Analysis of Integrated System Process Design

Hydrogen is conventionally produced by steam reforming of natural gas (methane) and petroleum feedstocks (e.g. naphtha) in an industry standard process for generating hydrogen commercially. The hydrogen concentration in the syngas (a mixture of CO and H_2) produced by the reforming process is further increased by reacting CO with additional steam in the WGS reaction. Since the WGS reaction is limited by reaction equilibrium, it is typically conducted in two temperature stages, at 400 and 250 °C, respectively, to increase conversion of CO. Product hydrogen is then separated from other gas phase constituents, primarily carbon dioxide and steam, by an amine scrubbing process.

While steam reforming of methane (natural gas) is most commonly used in a large-scale, central, hydrogen manufacturing facility; for the emerging market and need for small-scale, distributed hydrogen production facilities (as envisioned in the current program), an autothermal reforming process is likely to be the process choice. In an autothermal reforming process, part of the fuel (natural gas) is first burned with air to generate sufficient heat and steam necessary for the steam reforming of the remaining fuel. The amount of natural gas combusted is determined by the heat and steam requirements for the overall process. This process has obvious advantages for a small-scale, distributed facility such as fewer number of process units in a compact process. No separate steam generation facility is needed in this process, making it suitable for a "small footprint" H_2 generation system. Furthermore, due to the smaller scale of H_2 production, a pressure-swing-adsorption (PSA)-based H_2 purification step is likely to be used instead of the amine scrubbing process typically used in a conventional steam reforming process.

Since air rather than oxygen is typically used in the autothermal reforming process, the H_2 content of the product stream is lower than in the steam methane reforming process, making its separation by a membrane process more attractive. Autothermal reforming process is therefore considered here to develop an appropriate integrated process utilizing the high-temperature polymer membrane being developed here. In an integrated membrane-based H_2 production process, a high-temperature PBI-based membrane may be used either (i) as a membrane reactor combining the low-temperature WGS reaction and H_2 purification steps or (ii) as simply a H_2 purification unit following a conventional low-temperature WGS reactor replacing the conventional PSA system. Figure 28 schematically shows the "conventional"

autothermal reforming process as well as a hydrogen transport membrane (HTM)-integrated autothermal process where the membrane is used as a membrane reactor.

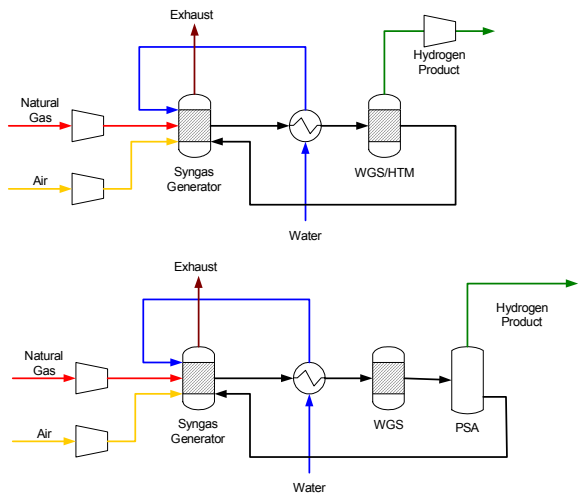

Figure 28. Schematics of membrane-integrated and conventional autothermal reforming processes.

In an autothermal reformer, the process variables are the methane to air and water ratios along with the reformer temperature and pressure. For a typical autothermal reformer operation at 100 psig pressure and 900 °C temperature and methane:air:water mole ratios of 3:5:2 , the equilibrium product gas composition exiting the reformer unit is shown in Table 19. For performing the membrane reactor/membrane separator simulations, the reformer product gas is assumed to be cooled to 300 °C in the heat exchanger shown in the schematics without any change in its composition. The PBI membrane permeability for H_2, CO, and CO_2 was measured at various temperatures and feed pressures in this program. The PBI membrane is also hydrophilic and highly permeable to water vapor, and the water vapor permeability in PBI had been determined in an earlier RTI study.[10] From these experimental data, the relative permeability of various gases to H_2 in the PBI membrane at 300 °C and 100 psig pressure was determined, as shown in Table 20. These values were used in conducting the process simulations.

Table 19. Product Syngas Composition Exiting Autothermal Reformer

Gas species	Mol%
H_2	45.8
CO	17.3
CO_2	2.0
CH_4	1.2
H_2O	6.8
N_2	26.9

Table 20. Relative Permeability of PBI Membrane for Various Gas Species to H_2

Gas species	Permeability relative to H_2
H_2	1
CO	0.025
CO_2	0.05
CH_4	0.025
H_2O	7
N_2	0.025

A high-temperature PBI membrane module may be used as a membrane reactor for conducting low-temperature WGS reaction with simultaneous H_2 separation or simply as a H_2 separation unit after conducting the WGS reaction in a conventional low-temperature reactor. A possible advantage of using the membrane module as a membrane reactor is to increase the yield of H_2 in the equilibrium-limited WGS reaction by removing one of the reaction products. Membrane module simulations were therefore conducted both (i) in the active membrane reactor mode as well as (ii) in the passive separation mode following a conventional reactor to determine CO conversion, H_2 recovery, permeate and residual gas compositions, and incremental relative membrane area as H_2 is removed along the length of the membrane reactor/separator. Equilibrium CO conversion in a conventional WGS reactor is assumed to determine the feed composition for the passive membrane separator module simulation. A simple one-dimensional equilibrium-based model[11] was used to conduct the model simulations. The model assumes dynamic equilibrium conditions at all locations along the membrane reactor/separator, and this would be a valid assumption for the low H_2 permeability of the PBI membrane.

The primary operating parameter in conducting WGS membrane reactor simulations is the steam-to-CO ratio in the feed gas to the membrane module. Table 19 provides the gas composition of the product syngas exiting the autothermal reformer. This syngas would be further mixed with additional steam to adjust the steam-to-CO ratio to a designated value model parameter. Simulations were conducted both in the active and passive modes for steam-to-CO ratios of 1:1, 1.5:1, and 2:1, respectively, using the relative permeability of each gas species noted in Table 20. Simulations assumed a constant membrane temperature of 300 °C and a constant feed pressure of 100 psig. The permeate pressure was assumed to be constant at 0 psig. The WGS reaction equilibrium constant at 300 °C is quite high at 41.2.

Relative membrane module areas required to achieve at least 80% net H_2 recovery in the permeate stream of the membrane module were determined from the model simulations. A net H_2 recovery is defined as the percentage of the maximum possible hydrogen (with complete conversion of CO) that is recovered in the permeate stream. Actual membrane module areas required to obtain 10 L(STP)/min H_2 flow in the permeate with 80% recovery of maximum possible H_2 were then determined for various steam-to-CO ratios in each of the two membrane simulation modes (passive vs. active) by using the experimentally determined H_2 permeance of 1.7×10^{-5} $cm^3(STP)/(cm^2 \cdot s \cdot cmHg)$ for the PBI membrane at 300 °C. The estimated membrane module areas ranged from 6 to 8 m^2 as shown in Figure 29.

For a given steam-to-CO ratio, the membrane area requirements for net 80% H_2 recovery were similar for both active and passive mode operations with the passive mode having a slightly lower area requirement. Utilization of the membrane module as a membrane reactor may still be advantageous because it combines the reactor and separator units into one. Increasing steam-to-CO ratio increased the equilibrium CO conversion and H_2 concentration, resulting in a reduction in required membrane area that appears to probably level off as the steam-to-CO ratio approaches 3.

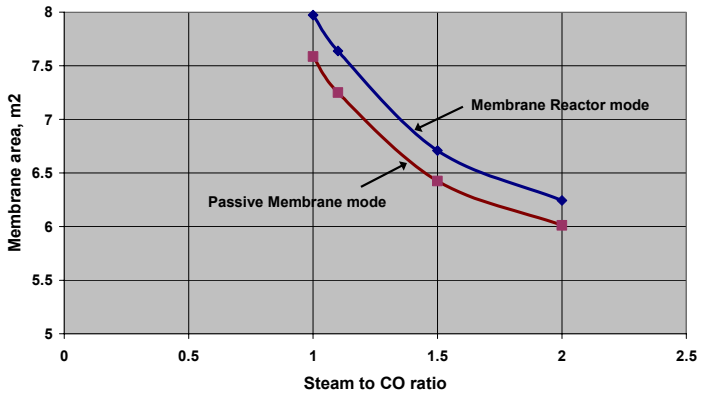

Figure 29. Estimated PBI membrane module area for 10 L(STP)/min of H_2 flow as a function of steam-to-CO ratio at 80% H_2 recovery.

The model simulation results using a steam-to-CO ratio of 1.0 for the membrane reactor and passive membrane separator modes are found in Figures 30 and 31, respectively. Similarly, Figures 32 and 33 present the simulation results based on a steam-to-CO ratio of 2.0 for the reactor and passive modes of operation, respectively. Because the PBI membrane is more permeable to water vapor than to H_2, using the membrane module as a membrane reactor did not indicate any increased CO conversion (Figures 30 and 32) as any advantage of product H_2 separation was offset by separation of water reactant as well. All simulations indicated a permeate H_2 concentration of 90-93% (dry basis) for a net H_2 recovery of 80%. Further purification of the product H_2 stream will therefore be necessary to condense out water and to remove CO before using the H_2, for example, in a polymer electrolyte membrane (PEM) fuel cell.

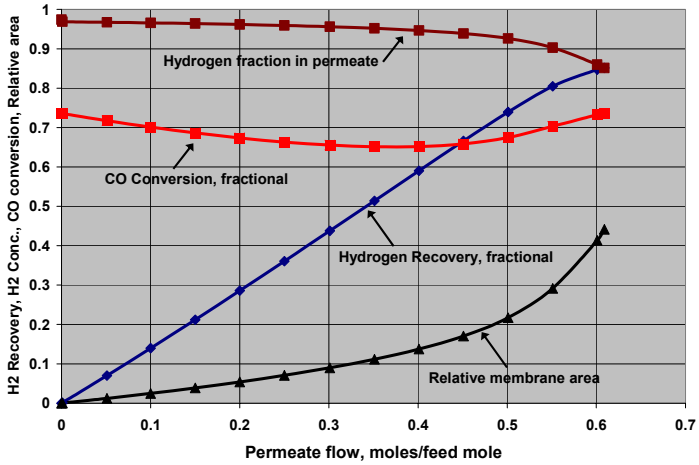

Figure 30. Process simulation using high-temperature PBI membrane in the *active* membrane reactor mode using a 1:1 steam-to-CO ratio.

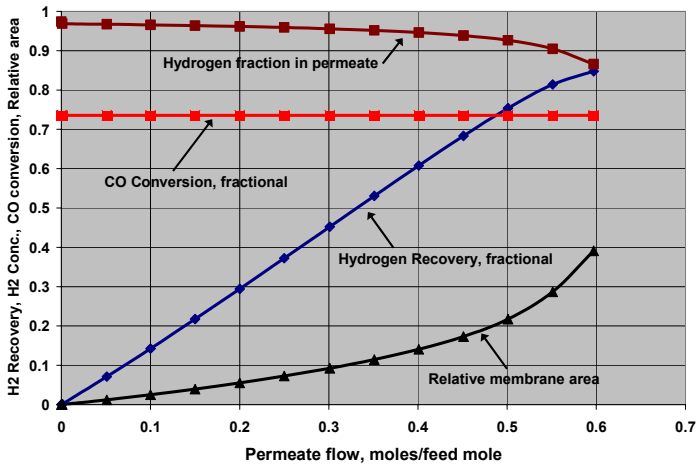

Figure 31. Process simulation using high-temperature PBI membrane in the *passive* separator mode using a 1:1 steam-to-CO ratio.

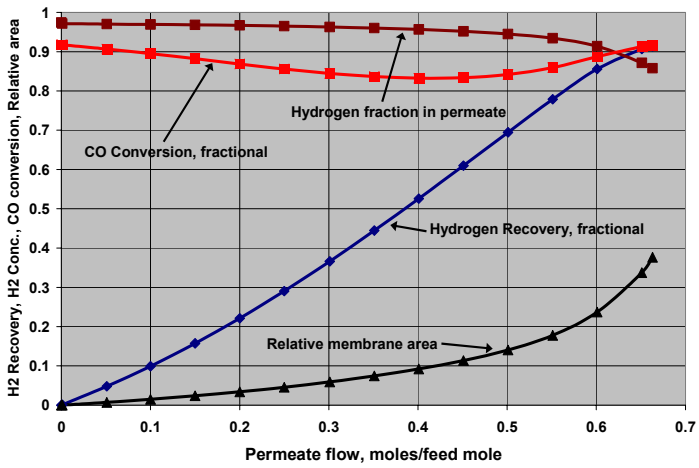

Figure 32. Process simulation using high-temperature PBI membrane in the *active* membrane reactor mode using a 2:1 steam-to-CO ratio.

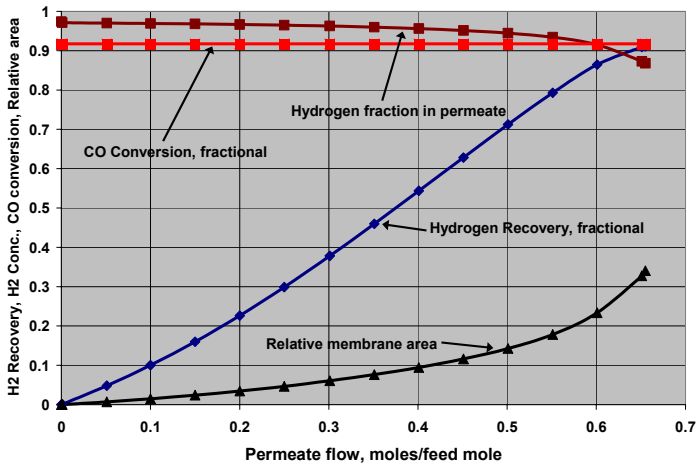

Figure 33. Process simulation using high-temperature PBI membrane in the *passive* separator mode using a 2:1 steam-to-CO ratio.

The H_2 permeability observed for the PBI membrane is typical of very highly thermally stable polymeric membranes. However, the PBI film was deposited on a porous stainless-steel-based AccuSep support tube for the single-tube test membrane module. Thus, the traditional advantage of a high surface area to volume ratio of a spiral wound or a hollow-fiber polymer membrane module is not available for the AccuSep-based PBI membrane module. Module simulations indicated that 6 to 8 m^2 PBI membrane area would be needed for a 10-L/min H_2 membrane module at 300 °C. The fabrication cost for AccuSep-based PBI membrane module must take into account the cost of the support tubes that is typically in the range of \$100 to 150/ft^2. The cost of preparing a PBI/AccuSep composite membrane would therefore be at least \$150/ft^2. The capital cost of a 7-m^2-area membrane module producing 10 L/min of H_2 would be about \$11,300, or about \$533/(ft^3/h H_2).

U.S. DOE has established hydrogen membrane module targets for metallic Pd-based membrane modules so these metallic membranes will be compared to the polymeric PBI membrane modules in our analysis here. The year 2010 targets for Pd-based membrane module costs and membrane hydrogen flux are \$1,000/ft^2 and 200 scfh/ft^2, respectively, at 400 °C and 20 psi transmembrane pressure differential. Combining these individual targets, the membrane module cost targets for a unit hydrogen capacity may be determined as \$5/(ft^3/h H_2). Clearly, an AccuSep support-based PBI membrane module is almost two orders of magnitude above the DOE's cost target, a large portion of which may be attributed to the AccuSep support itself. To realize the traditional advantages of polymeric membrane materials such as ease of processability, low-cost/high-volume processing, and high-surface-area packing density, the PBI membrane should be used in a polymer/polymer composite form. However, because traditional polymeric support media used for polymer/polymer composites are not suitable for high-temperature applications, efforts need to be directed toward the development of integrally skinned, asymmetric PBI membranes where a very thin (<1 μm), dense, selective PBI skin layer is mechanically supported on a bulk microporous structure formed from the PBI polymer itself. A detailed technical/economic analysis of the Accusep-supported PBI membrane module was not warranted and therefore not conducted here.

6. Conclusions and Future Work

A series of highly thermally stable polymer films was prepared from polymers that are among the most thermally stable polymeric materials known, and we mixed a variety of nanoparticles with them to explore the potential property-enhancing effects that nanoparticles have been shown to have on polymers in other applications. We characterized the polymers and nanocomposite film thermal stability properties to identify materials that were stable at conditions similar to those of the exit from the water gas shift reactor in a typical process train used to produce hydrogen from fossil fuels, such as coal. We determined that the presence of nanoparticles in poly(benzimidazole) (PBI) did not result in a decrease in thermal stability of the films. Moreover, we discovered certain combinations of nanoparticles that, when dispersed in PBI, actually improved its thermal stability in the presence of syngas containing H_2S. The permeation characteristics in pure gas measurements and mixed gas measurements were determined using relevant mixtures of H_2, CO, CO_2 and H_2S at temperatures up to 300°C. We prepared membranes that exhibited H_2/CO_2 selectivities in the range of 20 at 300°C and H_2/CO selectivities in the range of 35 at the same temperature. This combination of properties is considered good and is among the highest values reported for these gas pairs at such high temperatures. An economic analysis shows that the polymer membrane supported on a steel microporous support, which was the configuration considered in this study, would have significantly higher cost in practice than DOE's target for the cost of producing hydrogen using membranes. However, most of the cost comes from the current commercial cost of the steel microporous support. If an all-polymer membrane module could be developed, these cost estimates are likely to decrease dramatically.

References

(1) Lin, Y. S.; Kumakiri, I.; Nair, B. N.; Alsyouri, H. *Sep. Purif. Methods* **2002**, *31*, 229-379.

(2) Young, J. S. "CO_2 Separations Using High-Temperature Polymeric-Metallic Composite Membranes", Paper presented at the 2nd Annual Conference on Carbon Sequestration, Alexandria, VA, May 2003.

(3) Merkel, T. C.; He, Z.; Pinnau, I.; Freeman, B. D.; Meakin, P.; Hill, A. J. *Macromolecules* **2003**, *36*, 8406-8414.

(4) Merkel, T. C.; Freeman, B. D.; Spontak, R. J.; He, Z.; Pinnau, I.; Meakin, P.; Hill, A. J. *Science* **2002**, *296*, 519-522.

(5) Solvay. Application Bulletin Torlon AI-10 Polymer, Solvay Advanced Polymers, Atlanta, GA, 2001, pp 1-5.

(6) Mogri, Z.; Paul, D. R. *J. Membr. Sci.* **2000**, *175*(2), 253-265.

(7) Lin, H.; Freeman, B. D. *J. Membr. Sci.* **2004**, *239*, 105-117.

(8) Vu, D. Q.; Koros, W. J.; Miller, S. J. *J. Membr. Sci.* **2003**, *211*, 311-334.

(9) Poling, B. E.; Prausnitz, J. M.; O'Connell, J. P. *The Properties of Gases and Liquids*, 5th ed.; McGraw-Hill: New York, 2000.

(10) Bondar, V.; Damle, A. "Water Permeation by PBI Membrane and Possible Applications", Project report prepared for Pall Corporation, East Hills, NY, December 2004.

(11) Damle, A. S.; Gangwal, S. K.; Venkataraman, V. K. *Gas Sep. Purif.* **1994**, *8*(2), 101-106.